AD-A130 956 RADIATION PATTERNS OF AN ANTENNA MOUNTED ON THE OFF-MID 1/1
SECTION OF AN ELLIPSOID(U) OHIO STATE UNIV COLUMBUS
ELECTROSCIENCE LAB J G KIM ET AL. JUN 83 ESL-714215-3
UNCLASSIFIED N00019-81-C-0424 F/G 20/14 NL

END
DATE
FILMED
8 83
DTIC

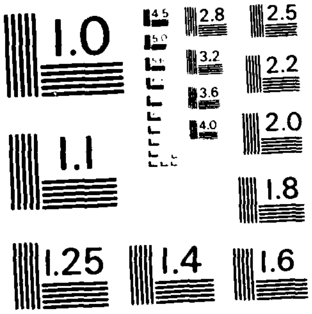
1.0
1.1
1.25
1.4
1.6
1.8
2.0
2.2
2.5
2.8
3.2
3.6
4.0
4.5
5.0

MICROCOPY RESOLUTION TEST CHART
NATIONAL BUREAU OF STANDARDS-1963-A

(12)

OSU

The Ohio State University

RADIATION PATTERNS OF AN ANTENNA MOUNTED ON THE OFF-MID SECTION OF AN ELLIPSOID

Jeung G. Kim
Walter D. Burnside

AD A130956

The Ohio State University
ElectroScience Laboratory
Department of Electrical Engineering
Columbus, Ohio 43212

DTIC
ELECTE
JUL 29 1983
S D
B

Quarterly Report 714215-3

Contract No. N00019-81-C-0424

June 1983

**APPROVED FOR PUBLIC RELEASE:
DISTRIBUTION UNLIMITED**

DTIC FILE COPY

Department of the Navy
Naval Air Systems Command
Washington, D.C. 20361

83 07 29 010

NOTICES

When Government drawings, specifications, or other data are used for any purpose other than in connection with a definitely related Government procurement operation, the United States Government thereby incurs no responsibility nor any obligation whatsoever, and the fact that the Government may have formulated, furnished, or in any way supplied the said drawings, specifications, or other data, is not to be regarded by implication or otherwise as in any manner licensing the holder or any other person or corporation, or conveying any rights or permission to manufacture, use, or sell any patented invention that may in any way be related thereto.

50272-101

REPORT DOCUMENTATION PAGE

1. REPORT NO. AD-A130 956

2.

3. Recipient's Accession No.

4. Title and Subtitle

RADIATION PATTERNS OF AN ANTENNA MOUNTED ON THE OFF-MID SECTION OF AN ELLIPSOID

5. Report Date June 1983

6.

7. Author(s)

Jeung G. Kim and Walter D. Burnside

8. Performing Organization Rept. No. ESL 714215-3

9. Performing Organization Name and Address

The Ohio State University ElectroScience Laboratory
Department of Electrical Engineering
Columbus, Ohio 43212

10. Project/Task/Work Unit No.

11. Contract(C) or Grant(G) No.

(C)

(G) N00019-81-C-0424

12. Sponsoring Organization Name and Address

Department of the Navy
Naval Air Systems Command
Washington, D.C. 20361

13. Type of Report & Period Covered

Quarterly Report

14.

15. Supplementary Notes

([illegible] ([illegible]) [illegible])

16. Abstract (Limit: 200 words)

An efficient numerical solution for the high frequency radiation patterns of an Antenna mounted on the Off-Mid Section ($\theta_s \neq 90°$) of an Ellipsoid is studied in this report. The Uniform Geometrical Theory of Diffraction (UTD) [1] is the basic approach applied here and the elliptic cone perturbation method ~~[2,3]~~ is used to simulate geodesic paths on the ellipsoid surface. The radiation patterns obtained using this technique are compared to those for prolate spheriod-mounted antennas, which have shown good agreement with measured data. Exact agreement between both results for typical spheroid geometries confirms that radiation patterns for ellipsoid mounted antennas can be solved efficiently by this numerical technique.

17. Document Analysis a. Descriptors

b. Identifiers/Open-Ended Terms

c. COSATI Field/Group

18. Availability Statement

APPROVED FOR PUBLIC RELEASE:
DISTRIBUTION UNLIMITED

19. Security Class (This Report) Unclassified

20. Security Class (This Page) Unclassified

21. No. of Pages 62

22. Price

(See ANSI-Z39.18) See Instructions on Reverse OPTIONAL FORM 272 (4-77)
(Formerly NTIS-35)
Department of Commerce

TABLE OF CONTENTS

Page

LIST OF FIGURES iii

I. INTRODUCTION 1

II. NUMERICAL TECHNIQUE 1

A. INTRODUCTION 1

B. NUMERICAL APPROACH FOR PATTERN CALCULATION 2

III. RESULTS 18

IV. CONCLUSIONS 21

REFERENCES 62

✓

Dist
A

LIST OF FIGURES

Figure		Page
1.	Geodesic path from the source on an ellipsoid.	3
2.	Geodesic path on a developed elliptic cone.	7
3.	Illustration of the diffraction point finding for a given receiver location.	15
4.	Illustration of the divergence factor ($\sqrt{d\psi_0/d\psi}$) terms.	17
5.	Definition of pattern axis.	19
6.	Various source locations tested.	20
7.	Comparison of radiation patterns for $R_t = 15\lambda$ for a short monopole mounted at $\phi_s = 0°$, $\theta_s = 60°$ on a $2\lambda \times 10\lambda$ spheriod.	23
8.	Comparison of radiation patterns for a short monopole mounted at $\phi_s = 0°$, $\theta_s = 30°$ on a $2\lambda \times 10\lambda$ spheriod.	25
9.	Comparison of radiation patterns for a short monopole mounted at $\phi_s = 30°$, $\theta_s = 60°$ on a $2\lambda \times 10\lambda$ spheriod.	27
10.	Comparison of radiation patterns for a short monopole mounted at $\phi_s = 30°$, $\theta_s = 30°$ on a $2\lambda \times 10\lambda$ spheriod.	29
11.	Comparison of radiation patterns for a short monopole mounted at $\phi_s = 30°$, $\theta_s = 120°$ on a $2\lambda \times 10\lambda$ spheriod.	31
12.	Comparison of radiation patterns for an axial slot mounted at $\phi_s = 0°$, $\theta_s = 60°$ on a $2\lambda \times 10\lambda$ spheriod.	33

Figure Page

13. Comparison of radiation patterns for an axial slot mounted at $\phi_s = 0°$, $\theta_s = 30°$ on a $2\lambda \times 10\lambda$ spheriod. 35

14. Comparison of radiation patterns for an axial slot mounted at $\phi_s = 30°$, $\theta_s = 60°$ on a $2\lambda \times 10\lambda$ spheriod. 37

15. Comparison of radiation patterns for an axial slot mounted at $\phi_s = 30°$, $\theta_s = 30°$ on a $2\lambda \times 10\lambda$ spheriod. 39

16. Comparison of radiation patterns for a circumferential slot mounted at $\phi_s = 0°$, $\theta_s = 60°$ on a $2\lambda \times 10\lambda$ spheriod. 41

17. Comparison of radiation patterns for a circumferential slot mounted at $\phi_s = 0°$, $\theta_s = 30°$ on a $2\lambda \times 10\lambda$ spheriod. 43

18. Comparison of radiation patterns for a circumferential slot mounted at $\phi_s = 30°$, $\theta_s = 60°$ on a $2\lambda \times 10\lambda$ spheriod. 45

19. Comparison of radiation patterns for a circumferential slot mounted at $\phi_s = 30°$, $\theta_s = 30°$ on a $2\lambda \times 10\lambda$ spheriod. 47

20. Radiation patterns for $R_t = 15\lambda$ for a short monopole mounted at $\phi_s = 0°$, $\theta_s = 60°$ on a $2\lambda \times 4\lambda \times 10\lambda$ ellipsoid. 49

21. Radiation patterns for a short monopole mounted at $\phi_s = 0°$, $\theta_s = 30°$ on a $2\lambda \times 4\lambda \times 10\lambda$ ellipsoid. 50

22. Radiation patterns for a short monopole mounted at $\phi_s = 30°$, $\theta_s = 60°$ on a $2\lambda \times 4\lambda \times 10\lambda$ ellipsoid. 51

23. Radiation patterns for a short monopole mounted at $\phi_s = 30°$, $\theta_s = 30°$ on a $2\lambda \times 4\lambda \times 10\lambda$ ellipsoid. 52

24. Radiation patterns for an axial slot mounted at $\phi_s = 0°$, $\theta_s = 60°$ on a $2\lambda \times 4\lambda \times 10\lambda$ ellipsoid. 53

Figure		Page
25.	Radiation patterns for an axial slot mounted at $\phi_s = 0°$, $\theta_s = 30°$ on a $2\lambda \times 4\lambda \times 10\lambda$ ellipsoid.	54
26.	Radiation patterns for an axial slot mounted at $\phi_s = 30°$, $\theta_s = 60°$ on a $2\lambda \times 4\lambda \times 10\lambda$ ellipsoid.	55
27.	Radiation patterns for an axial slot mounted at $\phi_s = 30°$, $\theta_s = 30°$ on a $2\lambda \times 4\lambda \times 10\lambda$ ellipsoid.	56
28.	Radiation patterns for a circumferential slot mounted at $\phi_s = 0°$, $\theta_s = 60°$ on a $2\lambda \times 4\lambda \times 10\lambda$ ellipsoid.	57
29.	Radiation patterns for a circumferential slot mounted at $\phi_s = 0°$, $\theta_s = 30°$ on a $2\lambda \times 4\lambda \times 10\lambda$ ellipsoid.	58
30.	Radiation patterns for a circumferential slot mounted at $\phi_s = 30°$, $\theta_s = 60°$ on a $2\lambda \times 4\lambda \times 10\lambda$ ellipsoid.	59
31.	Radiation patterns for a circumferential slot mounted at $\phi_s = 30°$, $\theta_s = 30°$ on a $2\lambda \times 4\lambda \times 10\lambda$ ellipsoid.	60
32.	Cone boundary used to define terms to be included in the shadow region.	61

I. INTRODUCTION

In applying the Uniform Geometrical Theory of Diffraction (UTD) to antenna radiation problem involving curved surfaces, a major task is to determine the final diffraction point and the geodesic path on the curved surface. For the antennas mounted on the fuselage of an aircraft, the fuselage can be modeled as an ellipsoid in the UTD analysis. Geodesic paths on an ellipsoid have been studied in detail in References [2,3] using an elliptic cone perturbation method which is very efficient.

Using this perturbation method and another numerical technique, which will be given in this report, the radiation patterns for ellipsoid mounted antennas is efficiently obtained. The theoretical UTD concept to calculate actual radiation fields is given in References [1,2].

II. NUMERICAL TECHNIQUE

A. INTRODUCTION

The ellipsoid simulated by a perturbed elliptic cone model is examined here. Since the elliptic cone is a developable surface, geodesics can be easily obtained [2,3]. Given a radiation direction (θ_t, ϕ_t), one can find the final diffraction point (θ_Q, ϕ_Q) by following the geodesic path, step by step, until the geodesic tangent coincides with the radiation direction (θ_t, ϕ_t). This is a rather tedius and time consuming process if applied for each new radiation direction. Considering a new radiation direction, which does not deviate greatly from the previous direction, one should be able to develop a solution which uses the properties of the surface and the previous geodesic path to find the new diffraction point. Such an approach is attempted here to make this solution as efficient as possible.

Since the field decays exponentially along the ray path on the surface, it is assumed that only one or possibly two dominant rays exist in the problems treated. One is referred to References [2,3] for more details on this topic.

B. NUMERICAL APPROACH FOR PATTERN CALCULATION

Assuming the diffraction point is located at Q ($a \cos v_e \cos v_r$, $b \cos v_e \sin v_r$, $c \sin v_e$) and the field point at P ($R_t \sin \theta_t \cos \phi_t$, $R_t \sin \theta_t \sin \phi_t$, $R_t \cos \theta_t$), then at the diffraction point Q the radiation direction (θ_t, ϕ_t) should coincide with the geodesic tangent $\hat{t}$ as shown in Figure 1. Thus,

$$\hat{t} = \hat{x}\, t_x + \hat{y}\, t_y + \hat{z}\, t_z$$

$$= \hat{t}_1 \cos \beta + \hat{t}_e \sin \beta \quad ,$$

where

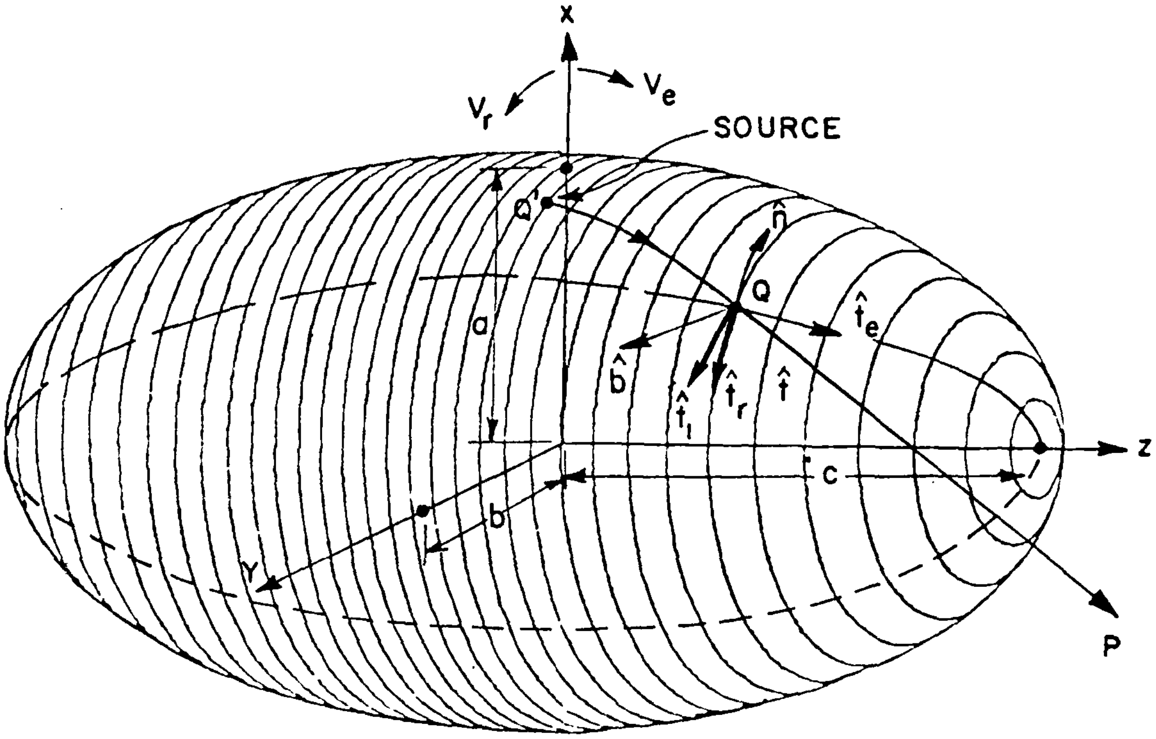
X
V_r
V_e
SOURCE
Q'
$\hat{n}$
Q
$\hat{t}_e$
a
$\hat{b}$
$\hat{t}_l$
$\hat{t}_r$
$\hat{t}$
Z
c
b
Y
P

Figure 1. Geodesic path from the source on an ellipsoid.

$$t_x = \frac{\sin\theta_t \cos\phi_t - \frac{a}{R_t}\cos v_e \cos v_r}{D}$$

$$t_y = \frac{\sin\theta_t \sin\phi_t - \frac{b}{R_t}\cos v_e \cos v_r}{D}$$

and

$$t_z = \frac{\cos\theta_t - \frac{c}{R_t}\sin v_e}{D} \quad .$$

Note that

$$D^2 = (\sin\theta_t\cos\phi_t - \frac{a}{R_t}\cos v_e\cos v_r)^2 + (\sin\theta_t\sin\phi_t$$

$$- \frac{b}{R_t}\cos v_e\sin v_r)^2 + (\cos\theta_t - \frac{c}{R_t}\sin v_e)^2$$

$$= 1 - 2[\sin\theta_t\cos v_e\ (\frac{a}{R_t}\cos\phi_t\cos v_r + \frac{b}{R_t}\sin\phi_t\sin v_r)$$

$$+ \frac{c}{R_t}\cos\theta_t\sin v_e] + [\cos^2 v_e\ (\frac{a^2}{R_t^2}\cos^2 v_r + \frac{b^2}{R_t^2}\sin^2 v_r) + \frac{c^2}{R_t^2}\sin^2 v_e]$$

, and

$$\hat{t}_1 = \hat{t}_e \times \hat{n}$$

$$= \frac{-\hat{x}a\sin v_r(b^2\sin^2 v_e + c^2\cos^2 v_e) + \hat{y}b\cos v_r(a^2\sin^2 v_e + c^2\cos^2 v_e)}{[a^2b^2\sin^2 v_e + c^2\cos^2 v_e(a^2\sin^2 v_r + b^2\cos^2 v_r)]^{1/2}} ---$$

$$--- \frac{+\hat{z}c(b^2 - a^2)\sin v_r\ \cos v_r\ \sin v_e\ \cos v_e}{[c^2\cos^2 v_e + \sin^2 v_e(a^2\cos^2 v_r + b^2\sin^2 v_r)]^{1/2}}$$

where

$$\hat{t}_e = \frac{\dfrac{\partial\vec{R}}{\partial v_e}}{\left|\dfrac{\partial\vec{R}}{\partial v_e}\right|} = \frac{-\hat{x}a \sin v_e \cos v_r - \hat{y}b \sin v_e \sin v_r + \hat{z}c \cos v_e}{[a^2\sin^2 v_e\cos^2 v_r+b^2\sin^2 v_e\sin^2 v_r+c^2\cos^2 v_e]^{1/2}}$$

$$\hat{t}_r = \frac{\dfrac{\partial\vec{R}}{\partial v_r}}{\left|\dfrac{\partial\vec{R}}{\partial v_r}\right|} = \frac{-\hat{x}a \cos v_e \sin v_r + \hat{y}b \cos v_e \cos v_r}{[a^2\cos^2 v_e\sin^2 v_r+b^2\cos^2 v_e\cos^2 v_r]^{1/2}}$$

and

$$n = \frac{\hat{t}_r \times \hat{t}_e}{|\hat{t}_r \times \hat{t}_e|}$$

$$= \frac{\hat{x}bc \cos v_e \cos v_r + \hat{y}ac \cos v_e \sin v_r + \hat{z}ab \sin v_e}{[a^2b^2\sin^2 v_e + c^2\cos^2 v_e(a^2\sin^2 v_r + b^2\cos^2 v_r)]^{1/2}} .$$

Equating the x-, y-, and z- components, respectively, one obtains

$$t_x = \frac{-a\sin v_r \cos\beta(b^2\sin^2 v_e + c^2\cos^2 v_e)}{[a^2b^2\sin^2 v_e+c^2\cos^2 v_e(a^2\sin^2 v_r+b^2\cos^2 v_r)]^{1/2}} \cdot$$

$$\cdot [c^2\cos^2 v_e+\sin^2 v_e(a^2\cos^2 v_r+b^2\sin^2 v_r)]^{1/2}$$

$$- \frac{a\sin v_e \cos v_r \sin\beta}{[c^2\cos^2 v_e+\sin^2 v_e(a^2\cos^2 v_r+b^2\sin^2 v_r)]^{1/2}}$$

$$= \frac{\sin\theta_t \cos\phi_t - \frac{a}{R_t} \cos v_e \cos v_r}{D} \quad . \qquad (1)$$

$$t_y = \frac{b\cos v_r \cos\beta(a^2\sin^2 v_e + c^2\cos v_e)}{[a^2b^2\sin^2 v_e + c^2\cos^2 v_e(a^2\sin^2 v_r + b^2\cos^2 v_r)]^{1/2} \cdot} $$

$$\cdot\ [c^2\cos^2 v_e + \sin^2 v_e(a^2\cos^2 v_r + b^2\sin^2 v_r)]^{1/2}$$

$$- \frac{b\sin v_e \sin v_r \sin\beta}{[c^2\cos^2 v_e + \sin^2 v_e(a^2\cos^2 v_r + b^2\sin^2 v_r)]^{1/2}}$$

$$= \frac{\sin\theta_t \sin\phi_t - \frac{b}{R_t}\cos v_e \sin v_r}{D} \quad . \qquad (2)$$

$$t_z = \frac{c(b^2-a^2)\sin v_r \cos v_r \sin v_e \cos v_e \cos\beta}{[a^2b^2\sin^2 v_e + c^2\cos^2 v_e(a^2\sin^2 v_r + b^2\cos^2 v_r)]^{1/2} \cdot}$$

$$\cdot\ [c^2\cos^2 v_e + \sin^2 v_e(a^2\cos^2 v_r + b^2\sin^2 v_r)]^{1/2}$$

$$+ \frac{c\cos v_e \sin\beta}{[c^2\cos^2 v_e + \sin^2 v_e(a^2\cos^2 v_r + b^2\sin^2 v_r)]^{1/2}}$$

$$= \frac{\cos\theta_t - \frac{c}{R_t}\sin v_e}{D} \quad . \qquad (3)$$

When the source is located at the off-mid section ($z \neq 0$ in Figure 1), the ellipsoid is modeled by a perturbed elliptic cone. The associated unfolded surface is shown in Figure 2(b). If γ and β denote the angle between $\hat{t}$ and $\hat{t}_1$ at Q' and Q, respectively, it is seen that $\beta = \gamma - \alpha$. With some manipulation, one can show that the perturbed geodesic path can be expressed as follows:

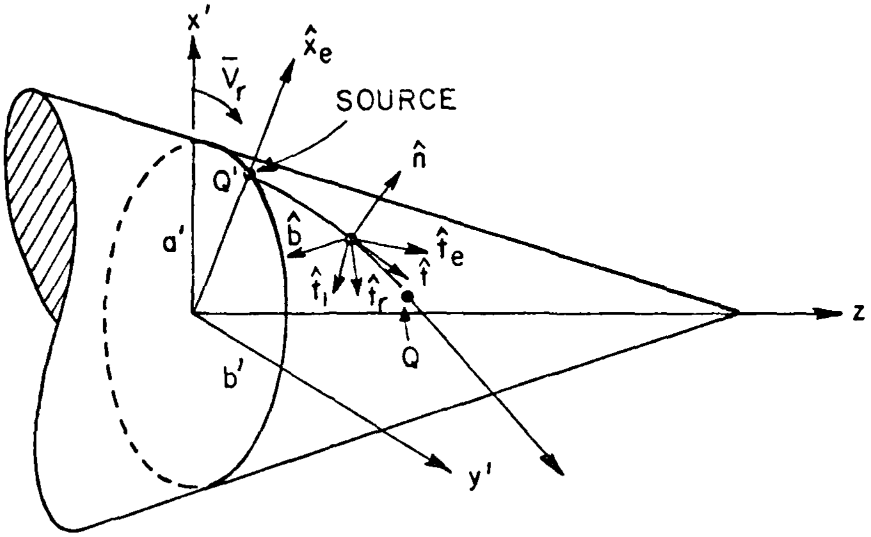
x'
V̄r
x̂e
SOURCE
Q'
n̂
b̂
t̂e
a'
t̂l
t̂r
t̂
Q
z
b'
y'

(a) TRUE ELLIPTIC CONE

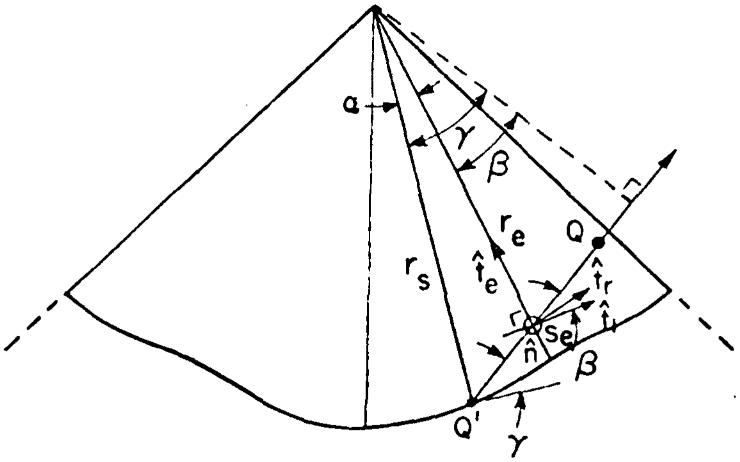
a
γ
β
re
Q
rs
t̂e
t̂r
t̂l
se
n̂
β
Q'
γ

(b) UNFOLDED PLANAR SURFACE

Figure 2. Geodesic path on a developed elliptic cone.

$$r_e \cos(\gamma-\alpha) = r_s \cos\gamma \tag{4}$$

where

$$\alpha(V_r) = \int_{V_{r_s}}^{V_r} \frac{[a_s^2 b_s^2 + Z_s^2 \cot^4 V_{e_s} (a_s^2 \sin^2 V_r' + b_s^2 \cos^2 V_r')]^{1/2}}{a_s^2 \cos^2 V_r' + b_s^2 \sin^2 V_r' + Z_s^2 \cot^4 V_{e_s}} \, dV_r' \quad ,$$

$$a_s = a\cos V_{e_s} \; , \; b_s = b\cos V_{e_s} \; , \; Z_s = c\sin V_{e_s} \quad ,$$

$$r_s = (a_s^2 \cos^2 V_{r_s} + b_s^2 \sin^2 V_{r_s} + Z_s^2 \cot^4 V_{e_s})^{1/2} \quad ,$$

$$r_e = (a_s^2 \cos^2 V_r + b_s^2 \sin^2 V_r + Z_s^2 \cot^4 V_{e_s})^{1/2} - S_e \quad ,$$

and

$$S_e = \int_{V_{e_s}}^{V_e} [c^2 \cos^2 V_e' + (a^2 \cos^2 V_r + b^2 \sin^2 V_r) \sin^2 V_e']^{1/2} dV_e' \quad .$$

Now, $[t_x (-b \sin V_r) + t_y a \cos V_r]$ yields

$$\frac{ab \cos(\gamma-\alpha) \, [c^2 \cos^2 V_e + \sin^2 V_e \, (a^2 \cos^2 V_r + b^2 \sin^2 V_r)]^{1/2}}{[a^2 b^2 \sin^2 V_e + c^2 \cos^2 V_e \, (a^2 \sin^2 V_r + b^2 \cos^2 V_r)]^{1/2}}$$

$$= \frac{\sin\theta_t \, (a\cos V_r \sin\phi_t - b\sin V_r \cos\phi_t)}{D} \quad . \tag{5}$$

Next, $\{[t_x b\cos V_r + t_y a\sin V_r] c\cos V_e + t_z ab\sin V_e\}$ yields

$$\frac{ab\sin V_e \cos\theta_t + c\sin\theta_t \cos V_e \,(a\sin\phi_t \sin V_r + b\cos\phi_t \cos V_r)}{D}$$

$$- \frac{abc}{DR_t} = 0 \quad . \tag{6}$$

Three functions can, then, be constructed as follows from Equations (4)-(6):

$$F(V_e, V_r, \gamma) = r_e\cos(\gamma-\alpha) - r_s\cos\gamma = 0 \quad . \tag{7}$$

$$G(R_t,\ \theta_t,\ \phi_t,\ V_e,\ V_r,\ \gamma)$$

$$= Dab\cos(\gamma-\alpha)[c^2\cos^2 V_e + \sin^2 V_e(a^2\cos^2 V_r + b^2\sin^2 V_r)]^{1/2}$$

$$- \sin\theta_t\ (a\sin\phi_t\ \cos V_r - b\cos\phi_t\ \sin V_r)\ \cdot$$

$$\cdot\ [a^2b^2\sin^2 V_e + c^2\cos^2 V_e\ (a^2\sin^2 V_r + b^2\cos^2 V_r)]^{1/2}$$

$$= 0 \quad . \tag{8}$$

Further, one finds that

$$H(R_t,\ \theta_t,\ \phi_t,\ V_e,\ V_r)$$

$$= ab\sin V_e\ \cos\theta_t + c\sin\theta_t\ \cos V_e\ (a\sin\phi_t\ \sin V_r + b\cos\phi_t\ \cos V_r)$$

$$- \frac{abc}{R_t} = 0 \quad . \tag{9}$$

Provided that one has obtained a diffraction point (V_e, V_r) for a receiver location (R_t, θ_t, ϕ_t), a numerical technique can now be developed from Equations (7), (8), and (9) to solve for ($V_e + \Delta V_e$, $V_r + \Delta V_r$) associated with a new receiver location ($R_t + \Delta R_t$, $\theta_t + \Delta\theta_t$, $\phi_t + \Delta\phi_t$). Assuming that the ith set of (R_t, θ_t, ϕ_t, V_e, V_r) is first known to satisfy $F_i = H_i = G_i = 0$, or at least approximately so, the next set ($R_t + \Delta R_t$, $\theta_t + \Delta\theta_t$, $\phi_t + \Delta\phi_t$, $V_e + \Delta V_e$, $V_r + \Delta V_r$) is obtained by enforcing $F_{i+1} = H_{i+1} = G_{i+1} = 0$, such that

$$F_{i+1} = F_i + F_{V_e}\Delta V_e + F_{V_r}\Delta V_r + F_\gamma \Delta\gamma = 0 \quad ,$$

$$G_{i+1} = G_i + G_{V_e}\Delta V_e + G_{V_r}\Delta V_r + G_\gamma \Delta\gamma$$

$$+ G_{\theta_t}\Delta\theta_t + G_{\phi_t}\Delta\phi_t + G_{R_t}\Delta Rt = 0$$

and

$$H_{i+1} = H_i + H_{V_e}\Delta V_e + H_{V_r}\Delta V_r + H_{\theta_t}\Delta\theta_t$$

$$+ H_{\phi_t}\Delta\phi_t + H_{R_t}\Delta R_t = 0 \quad .$$

In matrix form, it is given by

$$\begin{bmatrix} F_{V_e} & F_{V_r} & F_\gamma \\ G_{V_e} & G_{V_r} & G_\gamma \\ H_{V_e} & H_{V_r} & 0 \end{bmatrix} \begin{bmatrix} \Delta V_e \\ \Delta V_r \\ \Delta\gamma \end{bmatrix} = \begin{bmatrix} -F_i \\ -G_i - G_{\theta_t}\Delta\theta_t - G_{\phi_t}\Delta\phi_t - G_{R_t}\Delta R_t \\ -H_i - H_{\theta_t}\Delta\theta_t - H_{\phi_t}\Delta\phi_t - H_{R_t}\Delta R_t \end{bmatrix} \quad . \tag{10}$$

Note that the partial derivations are given by the following:

$$F_{Ve} = -[c^2\cos^2V_e+(a^2\cos^2V_r+b^2\sin^2V_r)\sin^2V_e]^{1/2}\cos(\gamma-\alpha)$$

$$F_{Vr} = (b^2-a^2)\ \sin V_r\cos V_r \Big\{ \frac{\cos^2 Ve_s}{(a_s^2\cos^2V_r+b_s^2\sin^2V_r+Z_s^2\cot^4Ve_s)^{1/2}}$$

$$- \int_{Ve_s}^{V_e} \frac{\sin^2V_e'\ dV_e'}{[c^2\cos^2V_e'+(a^2\cos^2V_r+b^2\sin^2V_r)\sin^2V_e']^{1/2}} \Big\} \cos(\gamma-\alpha)$$

$$+ \frac{r_e\sin(\gamma-\alpha)[a_s^2b_s^2+Z_s^2\cot^4V_{e_s}\ (a_s^2\sin^2V_r+b_s^2\cos^2V_r)]^{1/2}}{a_s^2\cos^2V_r+b_s^2\sin^2V_r+Z_s^2\cot^4V_{e_s}}$$

$$F_\gamma = r_s\ \sin\ \gamma\ -\ r_e\ \sin\ (\gamma-\alpha)$$

$$G_{V_e} = \frac{Dab(a^2\cos^2V_r+b^2\sin^2V_r-c^2)\sin V_e\cos V_e\ \cos(\gamma-\alpha)}{[c^2\cos^2V_e+(a^2\cos^2V_r+b^2\sin^2V_r)\sin^2V_e]^{1/2}}$$

$$- \frac{\sin\theta_t(a\sin\phi_t\cos V_r-b\cos\phi_t\sin V_r)[a^2b^2-(a^2\sin^2V_r+b^2\cos^2V_r)c^2]\sin V_e\cos V_e}{[(a^2\sin^2V_r+b^2\cos^2V_r)c^2\cos^2V_e+a^2b^2\sin^2V_e]^{1/2}}$$

$$+ \frac{ab\cos(\gamma-\alpha)}{D}\ [c^2\cos^2V_e+(a^2\cos^2V_r+b^2\sin^2V_r)\sin^2V_e]^{1/2}\ \cdot$$

$$\cdot\ \Big\{ \frac{c^2-(a^2\cos^2V_r+b^2\sin^2V_r)}{R_t^2}\ \sin V_e\cos V_e$$

$$+ \sin\theta_t\sin V_e(\frac{a}{R_t}\ \cos\phi_t\cos V_r\ +\ \frac{b}{R_t}\ \sin\phi_t\sin V_r)\ -\ \frac{c}{R_t}\ \cos\theta_t\cos V_e \Big\}$$

$$G_{V_r} = \frac{Dab\ \cos(\gamma-\alpha)(b^2-a^2)\sin V_r\ \cos V_r\ \sin^2 V_e}{[c^2\cos^2 V_e+(a^2\cos^2 V_r+b^2\sin^2 V_r)\sin^2 V_e]^{1/2}}$$

$$+ Dab[c^2\cos^2 V_e+(a^2\cos^2 V_r+b^2\sin^2 V_r)\sin^2 V_e]^{1/2}\ \sin(\gamma-\alpha)\ \cdot$$

$$\cdot \frac{[a_s^2 b_s^2+Z_s^2\cot^4 V_{e_s}(a_s^2\sin^2 V_r+b_s^2\cos^2 V_r)]^{1/2}}{a_s^2\cos^2 V_r+b_s^2\sin^2 V_r+Z_s^2\cot^4 V_{e_s}}$$

$$+ \frac{\sin\theta_t(a\sin\phi_t\cos V_r-b\cos\phi_t\sin V_r)(b^2-a^2)\sin V_r\cos V_r c^2\cos^2 V_e}{[(a^2\sin^2 V_r+b^2\cos^2 V_r)c^2\cos^2 V_e+a^2b^2\sin^2 V_e]^{1/2}}$$

$$+ \sin\theta_t(a\sin\phi_t\sin V_r+b\cos\phi_t\cos V_r)[(a^2\sin^2 V_r+b^2\cos^2 V_r)\ \cdot$$

$$\cdot\ c^2\cos^2 V_e+a^2b^2\sin^2 V_e]^{1/2}$$

$$+ \frac{ab\cos(\gamma-\alpha)}{D}\ [c^2\cos^2 V_e+(a^2\cos^2 V_r+b^2\sin^2 V_r)\sin^2 V_e]^{1/2}\ \cdot$$

$$\cdot\ [\frac{(b^2-a^2)}{R_t^2}\sin V_r\cos V_r\cos^2 V_e-\sin\theta_t\cos V_e(\frac{b}{R_t}\sin\phi_t\cos V_r$$

$$-\frac{a}{R_t}\cos\phi_t\sin V_r)]$$

$$G_\gamma = -Dab\sin(\gamma-\alpha)[c^2\cos^2 V_e+(a^2\cos^2 V_r+b^2\sin^2 V_r)\sin^2 V_e]^{1/2}$$

$$G_{\theta_t} = -\cos\theta_t(a\sin\phi_t\cos V_r - b\cos\phi_t\sin V_r)\cdot$$

$$\cdot\,[(a^2\sin^2 V_r + b^2\cos^2 V_r)c^2\cos^2 V_e + a^2b^2\sin^2 V_e]^{1/2}$$

$$+\,\frac{ab\cos(\gamma-\alpha)}{D}\,[c^2\cos^2 V_e + (a^2\cos^2 V_r + b^2\sin^2 V_r)\sin^2 V_e]^{1/2}\cdot$$

$$\cdot\,\left\{\frac{c}{R_t}\sin\theta_t\sin V_e - \cos\theta_t\cos V_e\left(\frac{a}{R_t}\cos\phi_t\cos V_r + \frac{b}{R_t}\sin\phi_t\sin V_r\right)\right\}$$

$$G_{\phi_t} = -\sin\theta_t(a\cos\phi_t\cos V_r + b\sin\phi_t\sin V_r)\cdot$$

$$\cdot\,[(a^2\sin^2 V_r + b^2\cos^2 V_r)c^2\cos^2 V_e + a^2b^2\sin^2 V_e]^{1/2}$$

$$+\,\frac{ab\cos(\gamma-\alpha)}{D}\,[c^2\cos^2 V_e + (a^2\cos^2 V_r + b^2\sin^2 V_r)\sin^2 V_e]^{1/2}\cdot$$

$$\cdot\,\left\{\sin\theta_t\cos V_e\left(\frac{a}{R_t}\sin\phi_t\cos V_r - \frac{b}{R_t}\cos\phi_t\sin V_r\right)\right\}$$

$$G_{R_t} = \frac{ab}{D}\cos(\gamma-\alpha)[c^2\cos^2 V_e + (a^2\cos^2 V_r + b^2\sin^2 V_r)\sin^2 V_e]^{1/2}\cdot$$

$$\cdot\,\{[\sin\theta_t\cos V_e(a\cos\phi_t\cos V_r + b\sin\phi_t\sin V_r) + c\cos\theta_t\sin V_e]/R_t^2$$

$$-\,[\cos^2 V_e(a^2\cos^2 V_r + b^2\sin^2 V_r) + c^2\sin^2 V_e]/R_t^3\}\quad.$$

$$H_{V_e} = ab\cos V_e\cos\theta_t - c\sin V_e\sin\theta_t(a\sin\phi_t\sin V_r + b\cos\phi_t\cos V_r)$$

$$H_{V_r} = c\cos V_e\sin\theta_t\ (a\sin\phi_t\cos V_r - b\cos\phi_t\sin V_r)$$

$$H_\gamma = 0$$

$$H_\theta = -ab\sin V_e\sin\theta_t + c\cos V_e\cos\theta_t(a\sin\phi_t\sin V_r + b\cos\phi_t\cos V_r)$$

$$H_{\phi_t} = c\cos V_e\sin\theta_t\ (a\cos\phi_t\sin V_r - b\sin\phi_t\cos V_r)$$

and

$$H_{R_t} = \frac{abc}{R_t^2}\ .$$

It is seen that one can solve for (ΔV_e, ΔV_r, $\Delta\gamma$), for a known (ΔR_t, $\Delta\theta_t$, $\Delta\phi_t$), using Equation (10). To obtain a diffraction point (V_e, V_r) for a given receiver location (R_t, θ_t, ϕ_t), one can always assume the first diffraction point is at the source (V_e, V_r) = (V_{e_s}, V_{r_s}) with the radiation direction (θ_f, $\phi_f = \frac{\pi}{2}$) for the positive ray (in $\hat{Y}$ direction) or (θ_f, $\phi_f = \frac{3}{2}\pi$) for negative ray (in $-\hat{Y}$ direction), and gradually add the increments (ΔR_t, $\Delta\theta_t$, $\Delta\phi_t$) until the final radiation direction (θ_t, ϕ_t) is reached as shown in Figure 3. More detail on this topic is provided in Reference [4]. One need not start out from the source everytime, but obtains the new diffraction point directly from Equation (10), provided that the new receiver location does not deviate greatly from the previous direction.

After the geodesic path is determined, various other parameters associated with actual field calculation must be found. The Fock parameter ξ was calculated in Reference [2] as follows:

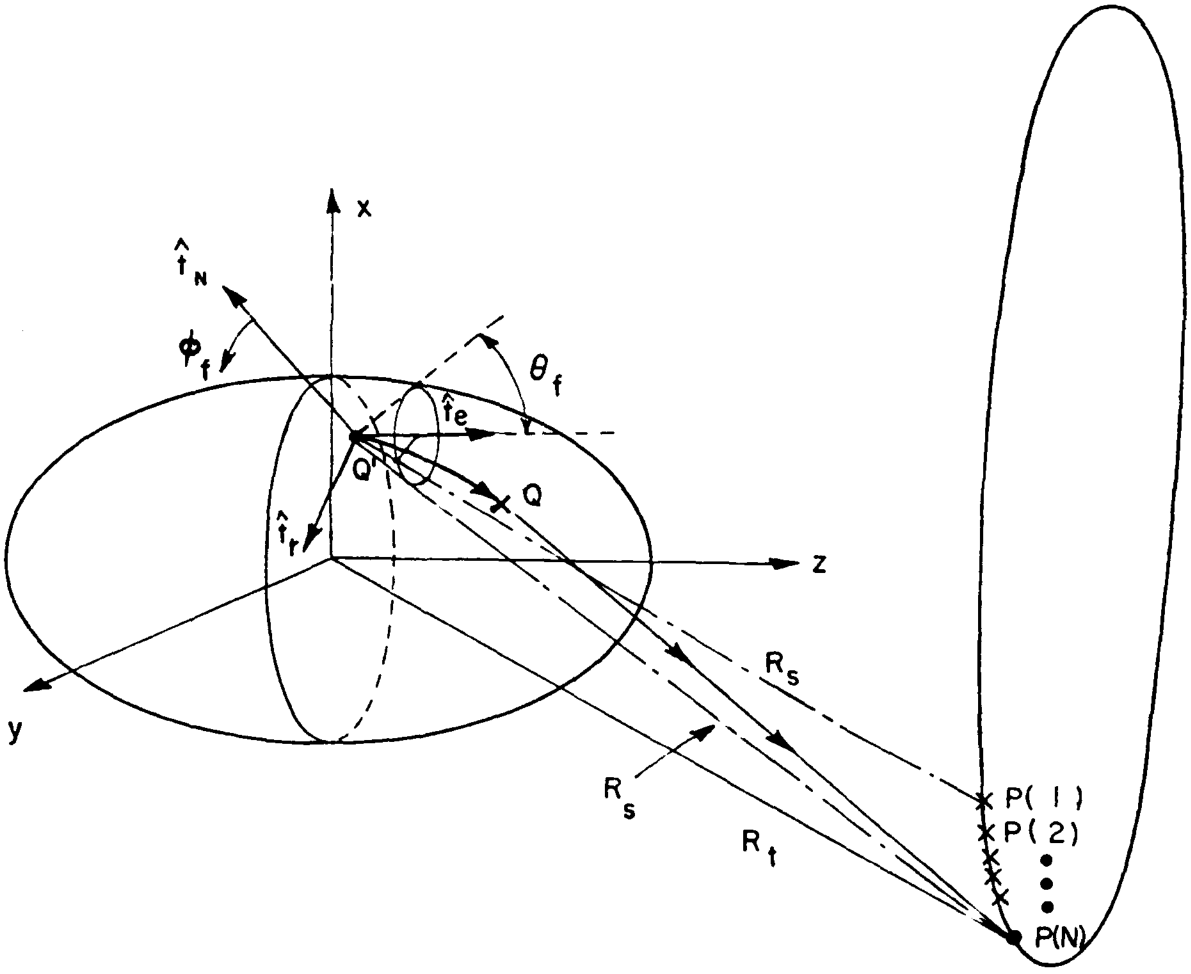

x
$\hat{t}_N$
ϕ_f
θ_f
$\hat{t}_e$
Q'
Q
$\hat{t}_r$
z
y
R_s
R_s
R_t
P(1)
P(2)
P(N)

Figure 3. Illustration of the diffraction point finding for a given receiver location.

$$\xi = r_s \cos\gamma \int_{V_{r_s}}^{V_r} \frac{1}{\rho_g} \left(\frac{k\rho_g}{2}\right)^{1/3} \frac{1}{\cos^2(\gamma-\alpha)} \frac{d\alpha}{dV_r'} dV_r'$$

where

$$\frac{d\alpha}{dV_r'} = \frac{[a_s^2 b_s^2 + Z_s^2 \cot^4 V_{e_s} \ (a_s^2 \sin^2 V_r' + b_s^2 \cos^2 V_r')]^{1/2}}{a_s^2 \cos^2 V_r' + b_s^2 \sin^2 V_r' + Z_s^2 \cot^4 V_{e_s}}$$

or

$$\xi = \int_{V_{e_s}}^{V_s} \frac{1}{\rho_g} \left(\frac{k\rho_g}{2}\right)^{1/3} \frac{1}{\sin(\gamma-\alpha)} \frac{dS_e}{dV_e'} d\ V_e' \qquad .$$

Note that $\rho_g = \dfrac{1}{k_1 \cos^2\beta + k_2 \sin^2\beta}$ and k_1 and k_2 are two principal curvatures.

Next, the ray divergence factor $\sqrt{\dfrac{d\psi_0(Q')}{d\psi(Q')}}$ is defined as the change in the separation of adjacent surface rays as shown in Figure 4. Since the ellipsoid simulating the aircraft fuselage will be long and slender, it is assumed that the ray divergence factor is unity in the analysis.

This completes the elliptic cone perturbation solution for the antenna mounted on the off-mid section of an ellipsoid.

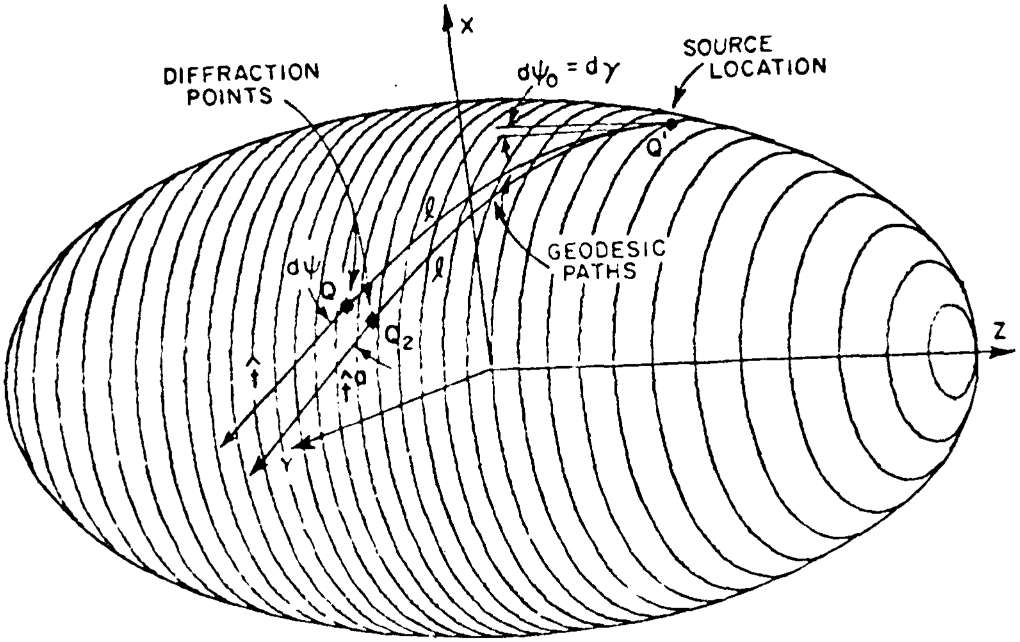
X
SOURCE LOCATION
$d\psi_0 = d\gamma$
DIFFRACTION POINTS
Q'
ℓ
ℓ
GEODESIC PATHS
$d\psi$
Q
Q_2
Z
$\hat{t}$
$\hat{a}$
$\hat{t}$
Y

Figure 4. Illustration of the divergence factor ($\sqrt{d\psi_0/d\psi}$) terms.

III. RESULTS

The solutions presented in the previous chapter are employed to compute the near field radiation patterns for short monopoles or slots mounted on an ellipsoid.

To examine different conical pattern cuts, a cartesian coordinate system (x',y',z') originally defining the ellipsoid geometry is now rotated into a new system (x,y,z) as shown in Figure 5. Note that the new cartesian coordinates are found by first rotating about the z'-axis a angle ϕ_c and then about the y-axis a angle θ_c. The pattern is, then, taken in the (x,y,z) coordinate system with θ_p fixed and ϕ_p varied.

To show the validity of the elliptic cone perturbation solution, some typical sources, i.e., short monopole, axial slot and circumferential slot, and various source locations are chosen as shown in Figure 6.

For each case the following typical radiation patterns are obtained:

a) $\theta_c = 0°$, $\phi_c = 90°$, $\theta_p = 90°$ (roll plane pattern)
b) $\theta_c = 30°$, $\phi_c = 90°$, $\theta_p = 90°$
c) $\theta_c = 60°$, $\phi_c = 90°$, $\theta_p = 90°$
d) $\theta_c = 90°$, $\phi_c = 90°$, $\theta_p = 90°$ (elevation plane pattern)
e) $\theta_c = 90°$, $\phi_c = 0°$, $\theta_p = 90°$ (azimuth plane pattern).

The radiation patterns obtained by the ellipsoid program, which uses an ellipsoid to simulate the aircraft fuselage, are compared to those obtained using the spheriod solution [5] in each case.

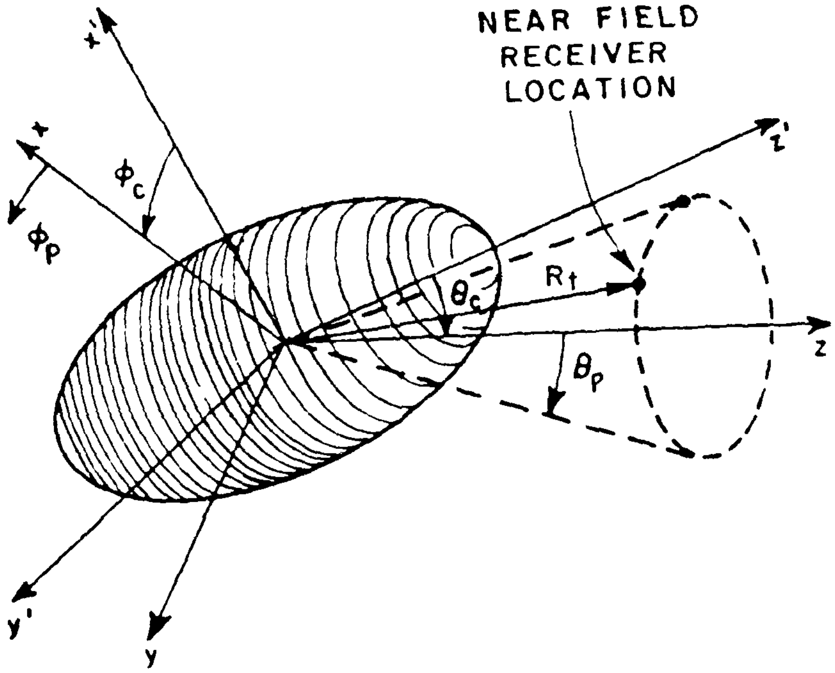

NEAR FIELD RECEIVER LOCATION
x'
x
ϕ_c
ϕ_p
z'
R_t
θ_c
z
θ_p
y'
y

Figure 5. Definition of pattern axis.

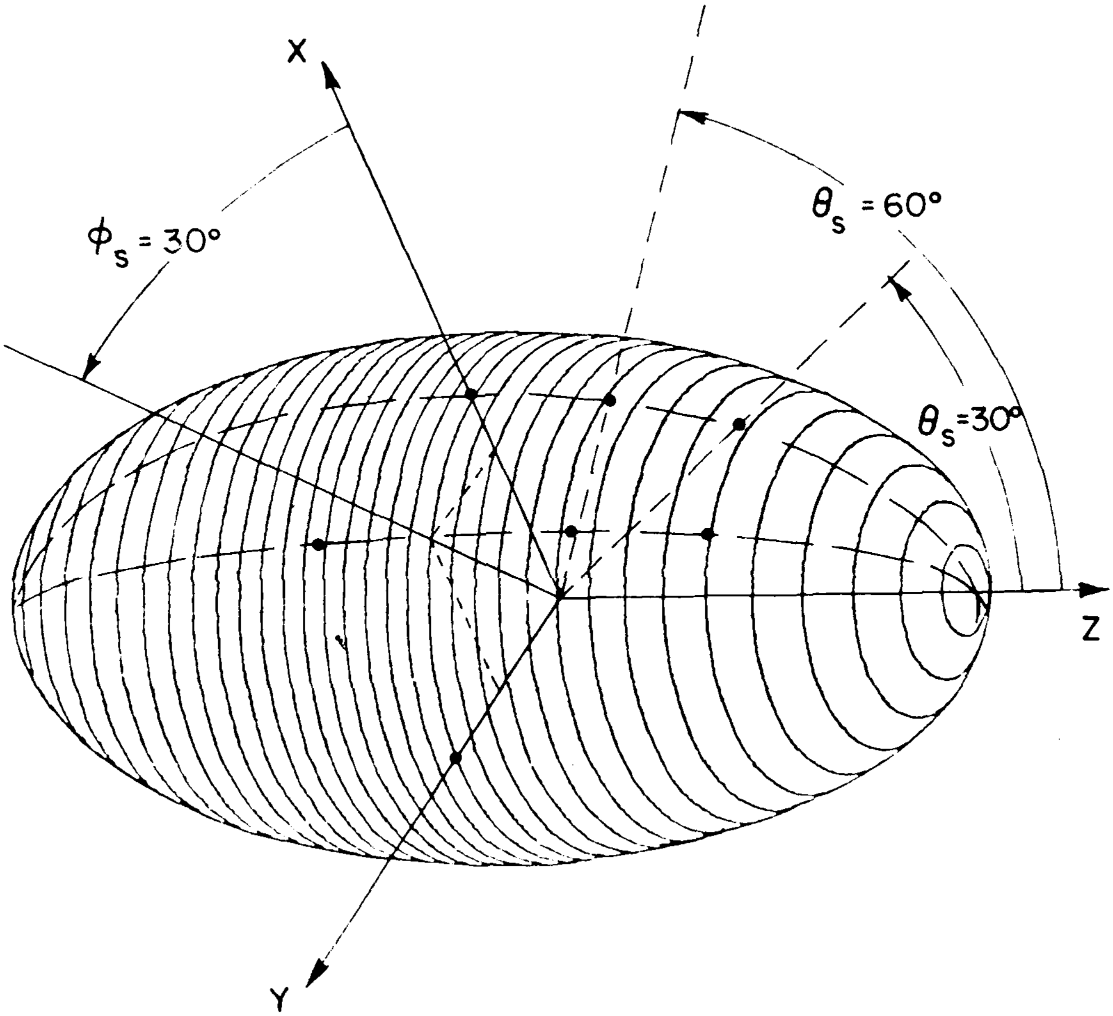
X
$\phi_s = 30°$
$\theta_s = 60°$
$\theta_s = 30°$
Z
Y

Figure 6. Various source locations tested.

It is noted that the geodesic tracing method of the ellipsoid program for the side mounted antennas (Figures 9, 10, 11, 14, 15, 18, 19) is different from that of the spheroid program because the ellipsoid is not a surface of revolution.

The exact agreement between the results of the ellipsoid program and the spheroid program as shown in Figures 7-19 gives one confidence about the validity of the elliptic cone technique.

Next, the ellipsoid program is employed to calculate the radiation patterns due to antennas mounted on an ellipsoid surface. The typical ellipsoid geometry ($2\lambda \times 4\lambda \times 10\lambda$) is chosen and examined for various sources and source locations.

The cone boundary shown in Figure 32 is used in determining whether one or two rays are used in the solution. Note that β_{12} is defined automatically by determining the caustic angle in the elevation pattern (β_c) and adding a few additional degrees to that value, i.e., $\beta_{12} = \beta_c + \Delta\beta$ where $2° \leq \Delta\beta \leq 10°$. One would expect to observe slight discontinuities somewhere, because various numbers of rays are included in different regions.

IV. CONCLUSIONS

The object of this study has been to develop an efficient numerical solution for the high frequency radiation patterns of an ellipsoid-mounted antenna. The UTD is used in this study to calculate the radiation patterns, and the elliptic cone perturbation method is applied to simulate the geodesic paths on the ellipsoid, which in turn can be used to model an aircraft or missile fuselage. For a given radiation direction in the shadow region, the geodesic path and final diffraction point on the ellipsoid can, then, be found via an efficient numerical approach.

The exact agreement of the radiation patterns from two different programs confirms that this elliptic cone perturbation solution is very useful in predicting the high frequency radiation patterns for antennas mounted on the off-mid section of an ellipsoid.

This numerical solution will be employed, along with flat plates to construct a general solution for calculating radiation patterns due to airborne antennas.

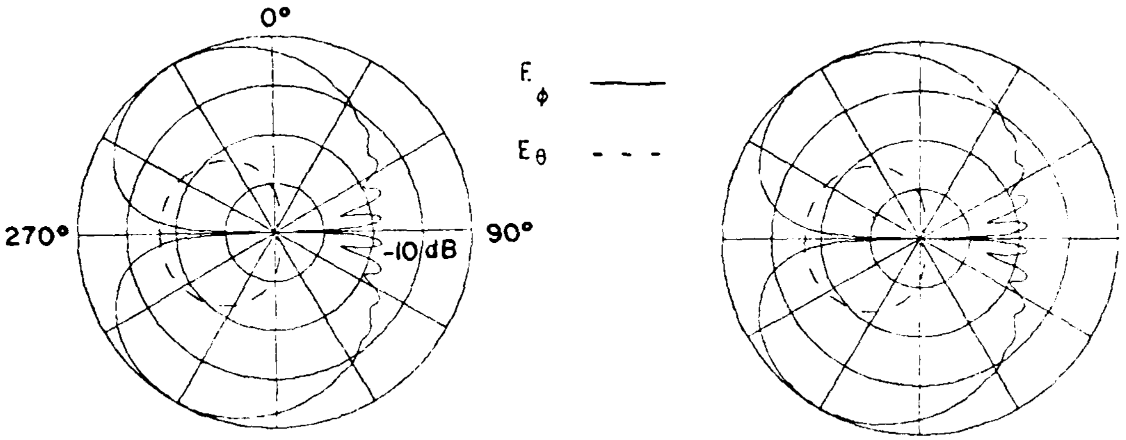

(a) $\theta_c = 0°, \phi_c = 90°, \theta_p = 90°$

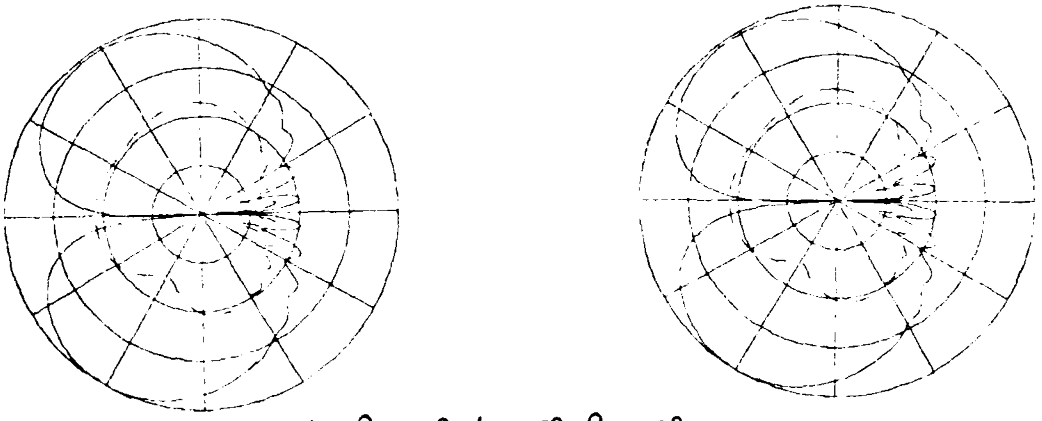

(b) $\theta_c = 30°, \phi_c = 90°, \theta_p = 90°$

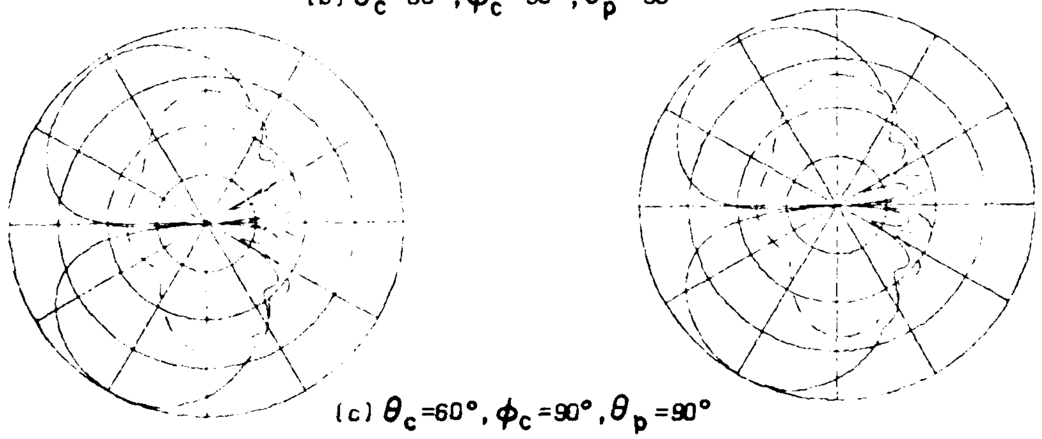

(c) $\theta_c = 60°, \phi_c = 90°, \theta_p = 90°$

Figure 7. Comparison of radiation patterns for $R_t = 15\lambda$ for a short monopole mounted at $\phi_s = 0°$, $\theta_s = 60°$ on a 2λ x 10λ spheriod.

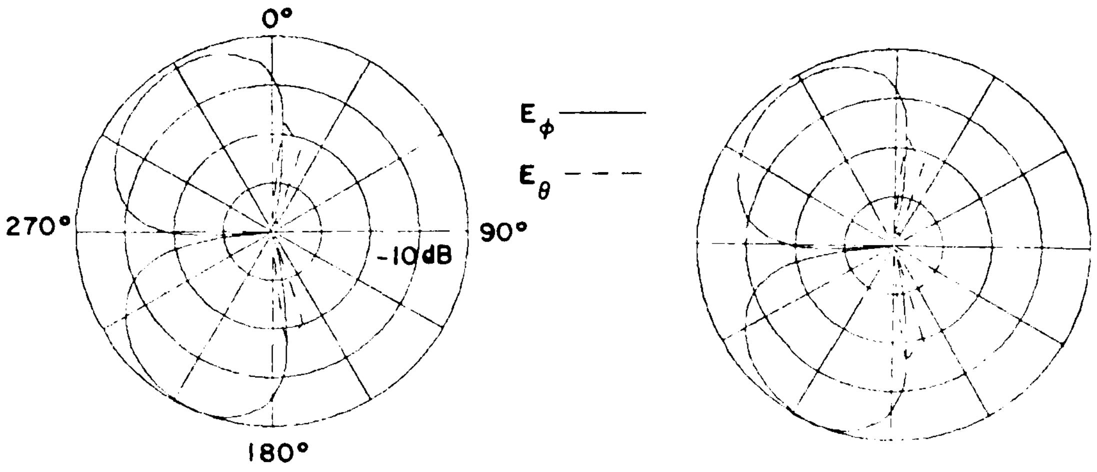

(d) $\theta_c = 90°, \phi_c = 90°, \theta_p = 90°$

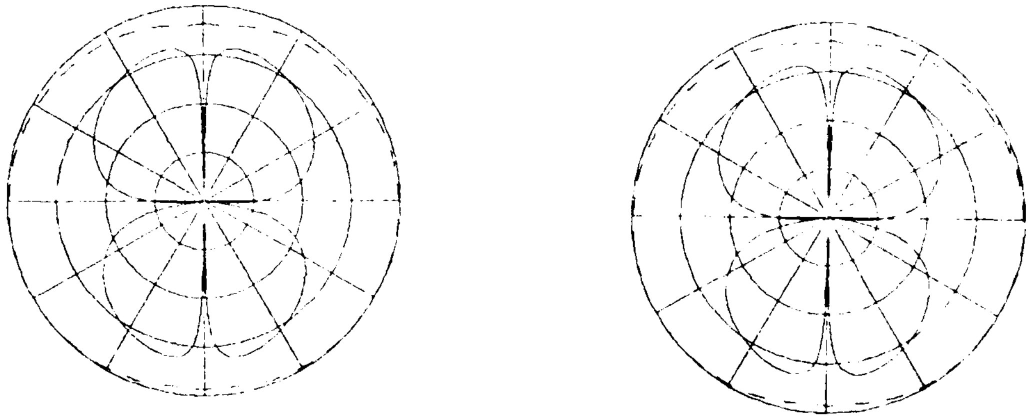

(e) $\theta_c = 90°, \phi_c = 0°, \theta_p = 90°$

Ellipsoid Program

Spheroid Program

Figure 7. (continued)

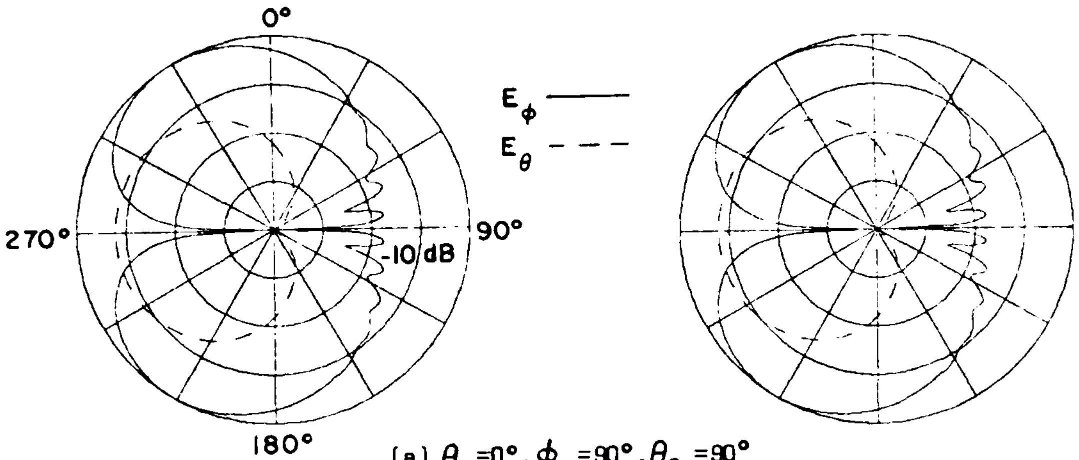

(a) $\theta_c = 0°$, $\phi_c = 90°$, $\theta_p = 90°$

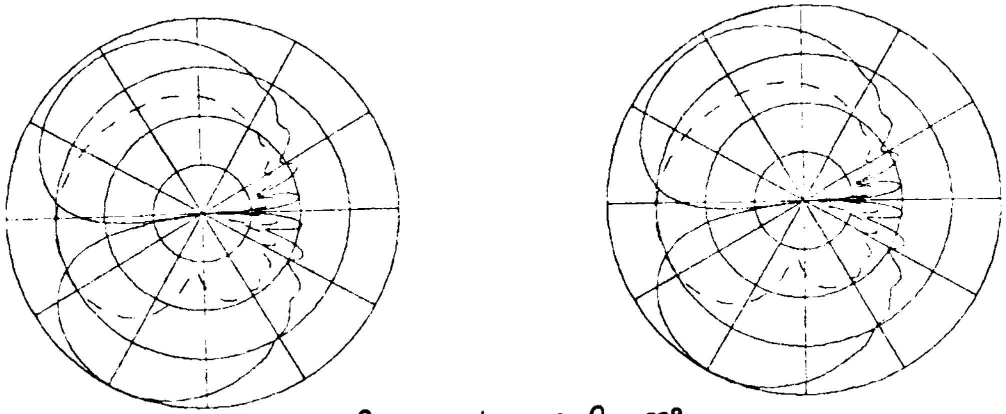

(b) $\theta_c = 30°$, $\phi_c = 90°$, $\theta_p = 90°$

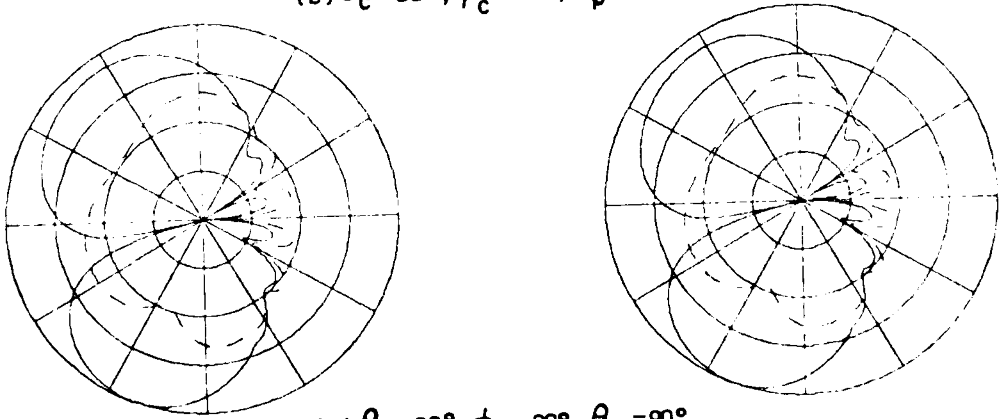

(c) $\theta_c = 60°$, $\phi_c = 90°$, $\theta_p = 90°$

Ellipsoid Program **Spheroid Program**

Figure 8. Comparison of radiation patterns for a short monopole mounted at $\phi_s = 0°$, $\theta_s = 30°$ on a $2\lambda \times 10\lambda$ spheriod.

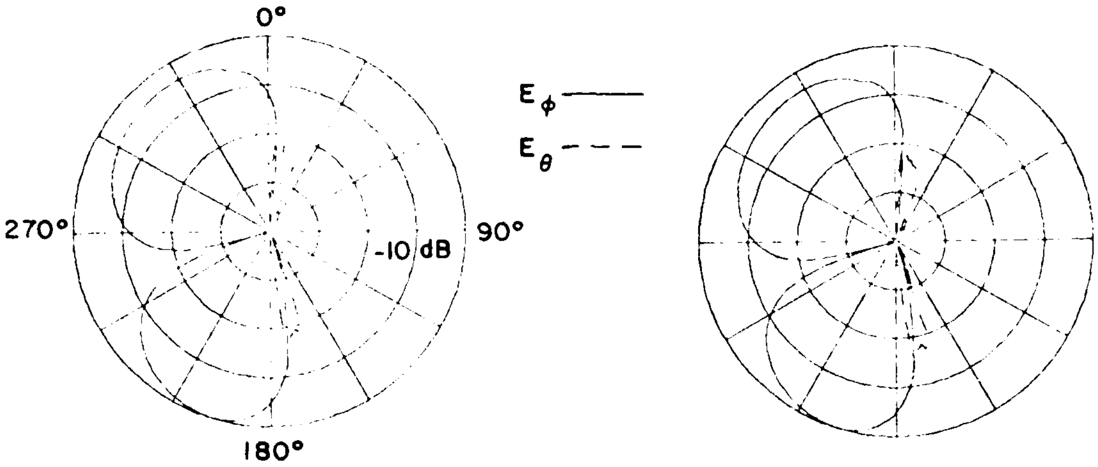

(d) $\theta_c = 90°$, $\phi_c = 90°$, $\theta_p = 90°$

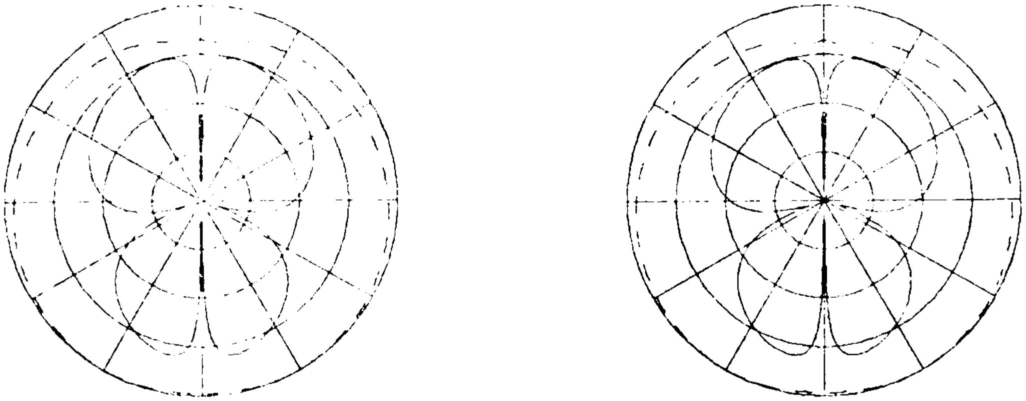

(e) $\theta_c = 90°$, $\phi_c = 0°$, $\theta_p = 90°$

Ellipsoid Program

Spheroid Program

Figure 8. (continued)

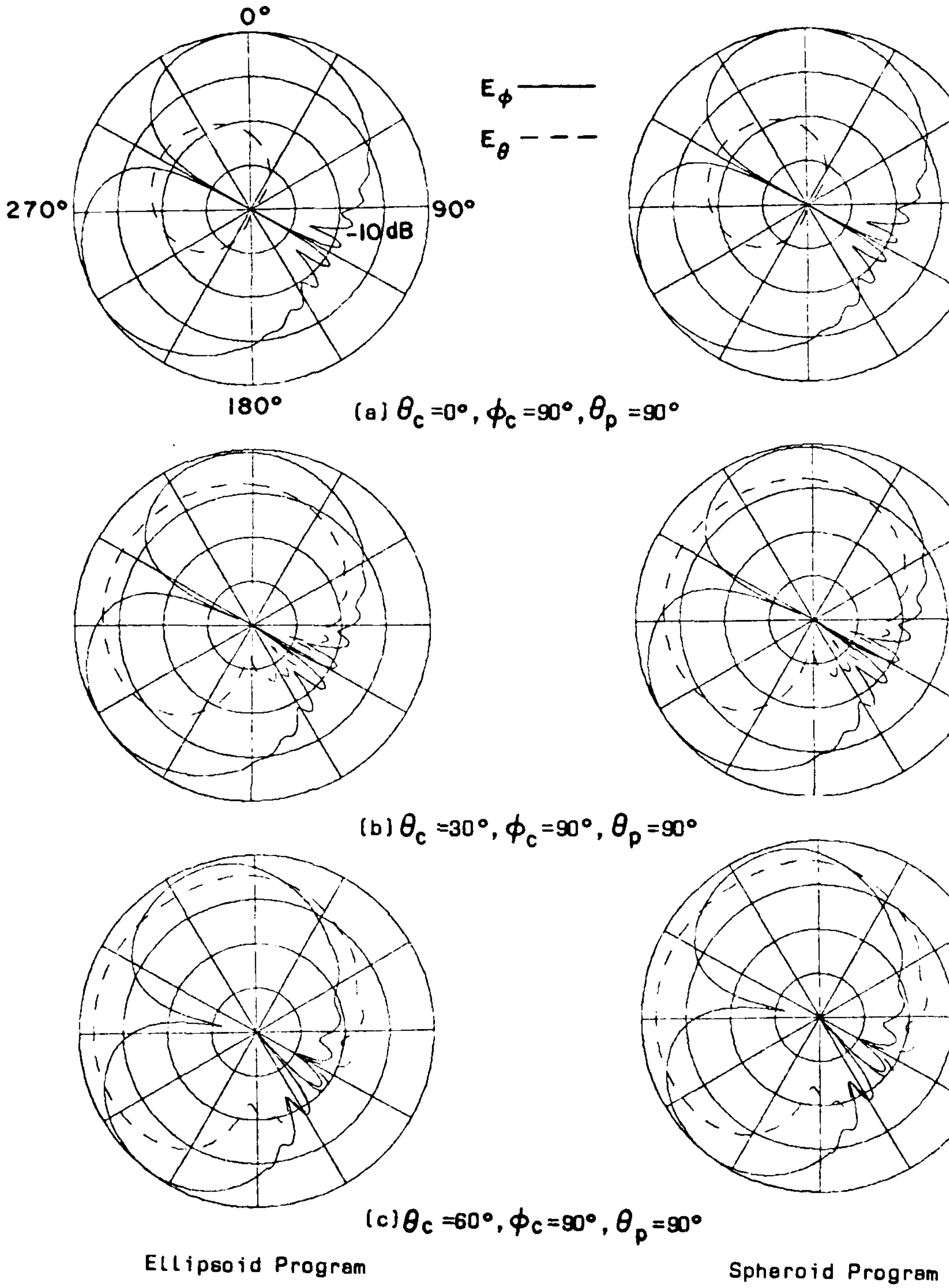

(a) $\theta_c = 0°$, $\phi_c = 90°$, $\theta_p = 90°$

(b) $\theta_c = 30°$, $\phi_c = 90°$, $\theta_p = 90°$

(c) $\theta_c = 60°$, $\phi_c = 90°$, $\theta_p = 90°$

Figure 9. Comparison of radiation patterns for a short monopole mounted at $\phi_s = 30°$, $\theta_s = 60°$ on a $2\lambda \times 10\lambda$ spheriod.

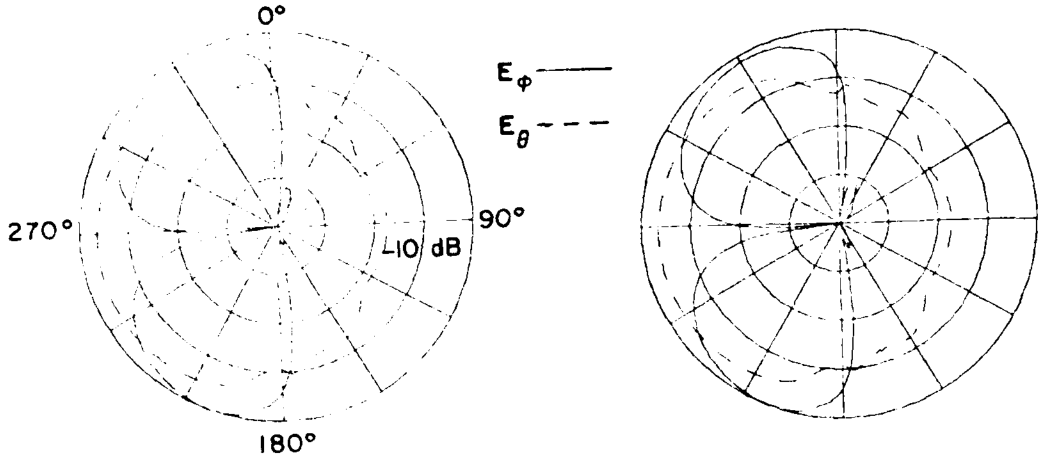

(d) $\theta_c = 90°, \phi_c = 90°, \theta_p = 90°$

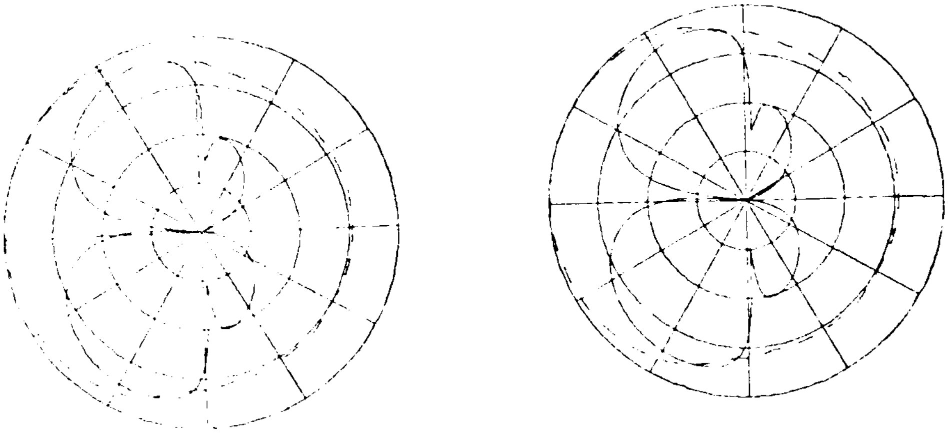

(e) $\theta_c = 90°, \phi_c = 0°, \theta_p = 90°$

Ellipsoid Program

Spheroid Program

Figure 9. (continued)

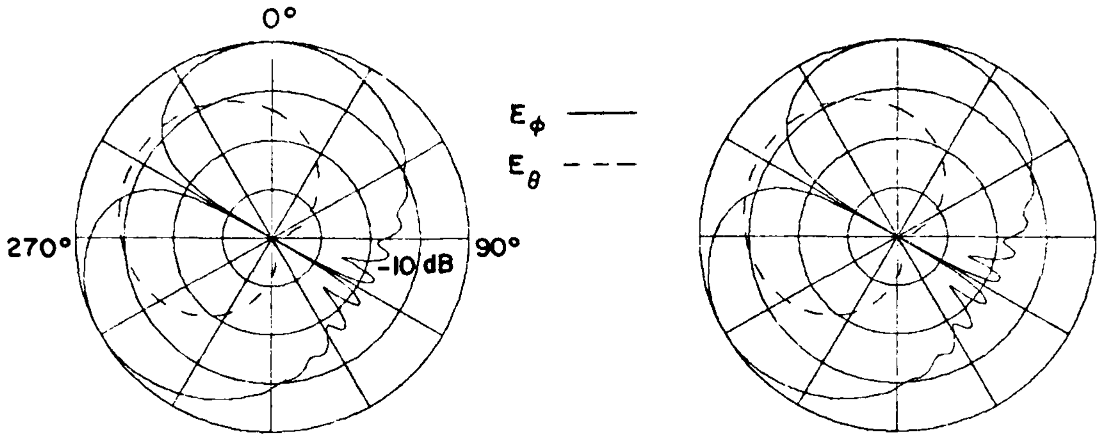

(a) $\theta_c = 0°, \phi_c = 90°, \theta_p = 90°$

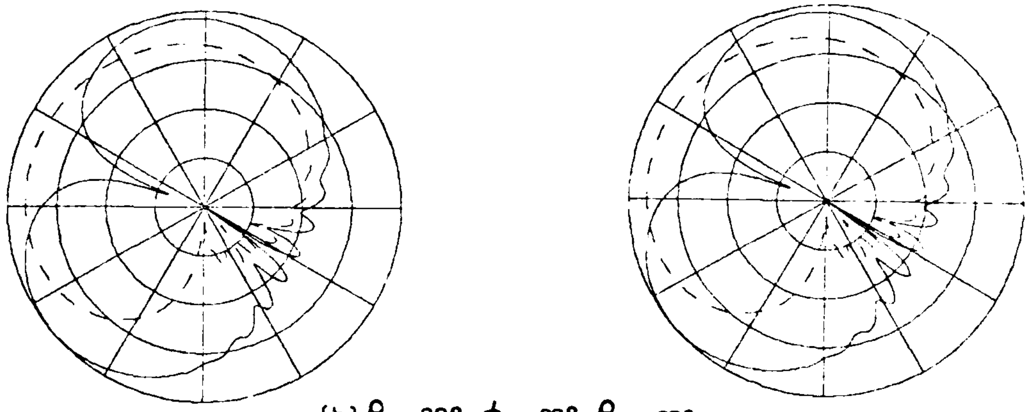

(b) $\theta_c = 30°, \phi_c = 90°, \theta_p = 90°$

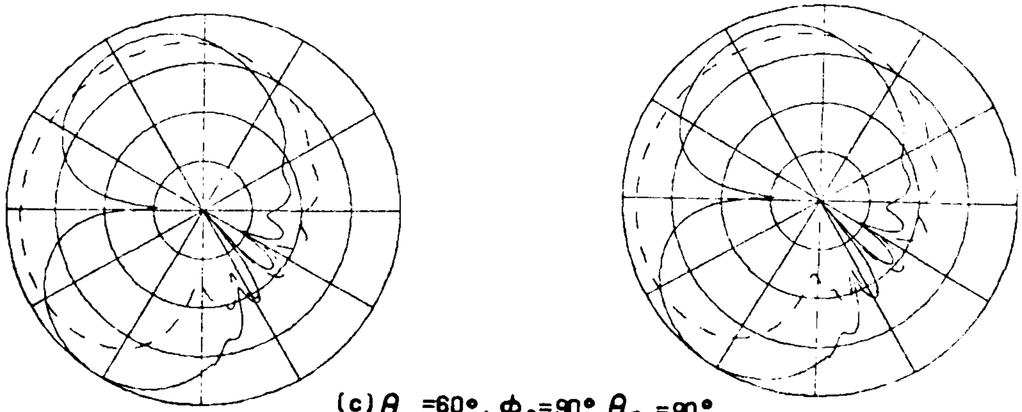

(c) $\theta_c = 60°, \phi_c = 90°, \theta_p = 90°$

Ellipsoid Program   Spheroid Program

Figure 10. Comparison of radiation patterns for a short monopole mounted at $\phi_s = 30°$, $\theta_s = 30°$ on a $2\lambda \times 10\lambda$ spheriod.

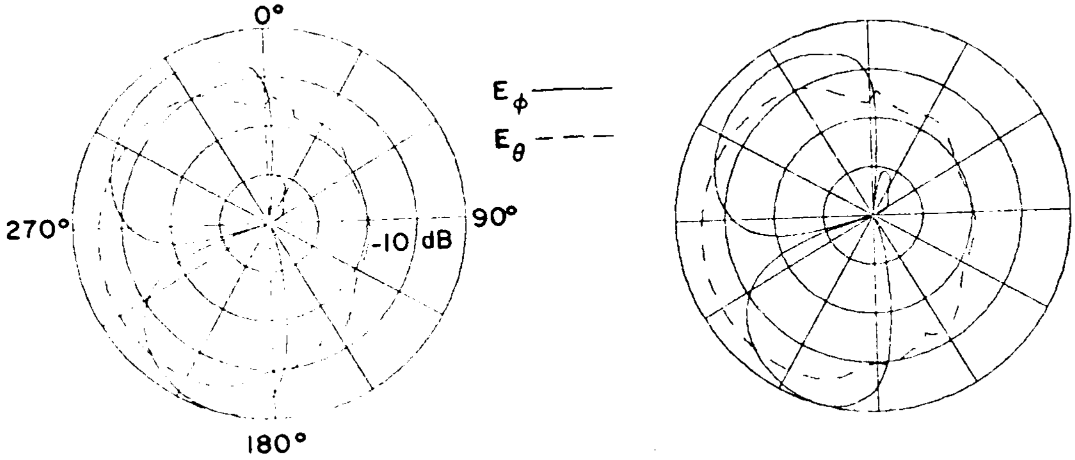

(d) $\theta_c = 90°$, $\phi_c = 90°$, $\theta_p = 90°$

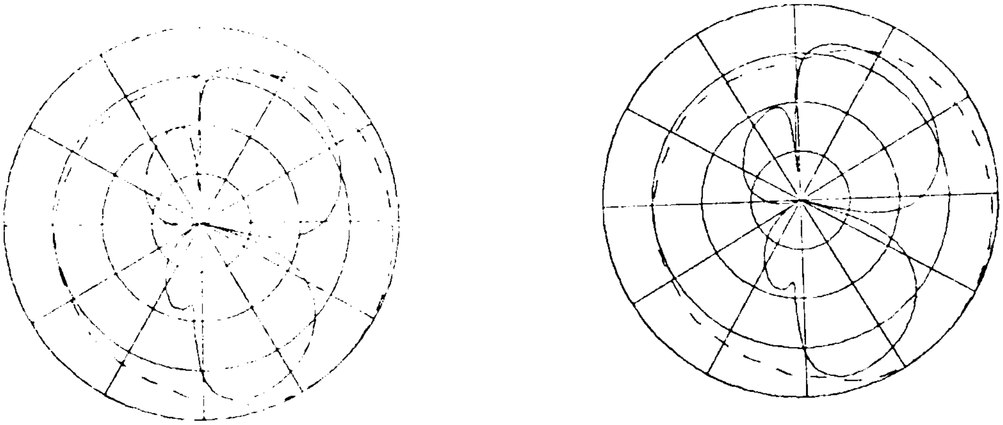

(e) $\theta_c = 90°$, $\phi_c = 0°$, $\theta_p = 90°$

Ellipsoid Program

Spheroid Program

Figure 10. (continued)

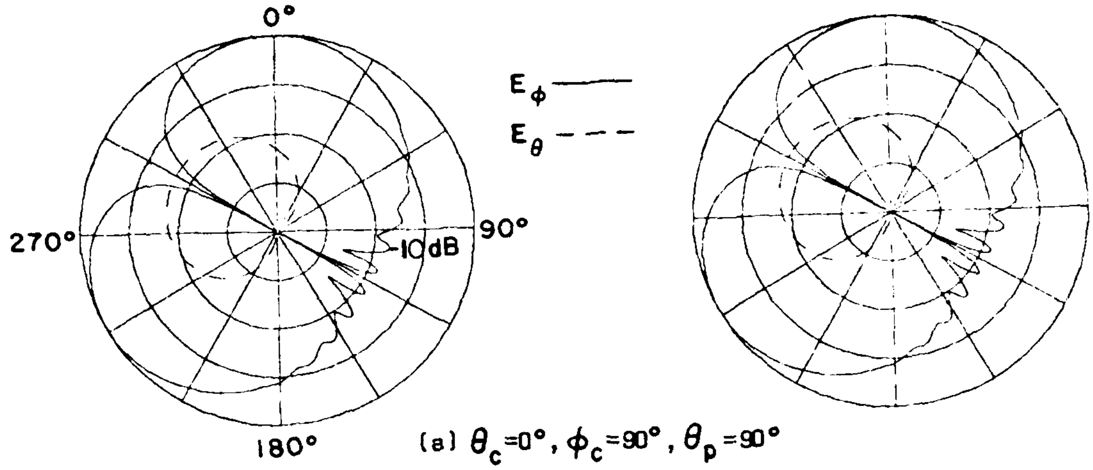

(a) $\theta_c = 0°$, $\phi_c = 90°$, $\theta_p = 90°$

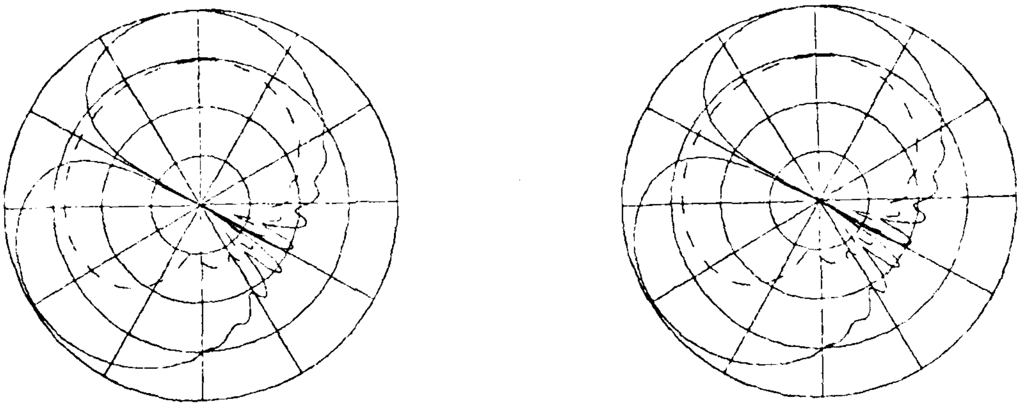

(b) $\theta_c = 30°$, $\phi_c = 90°$, $\theta_p = 90°$

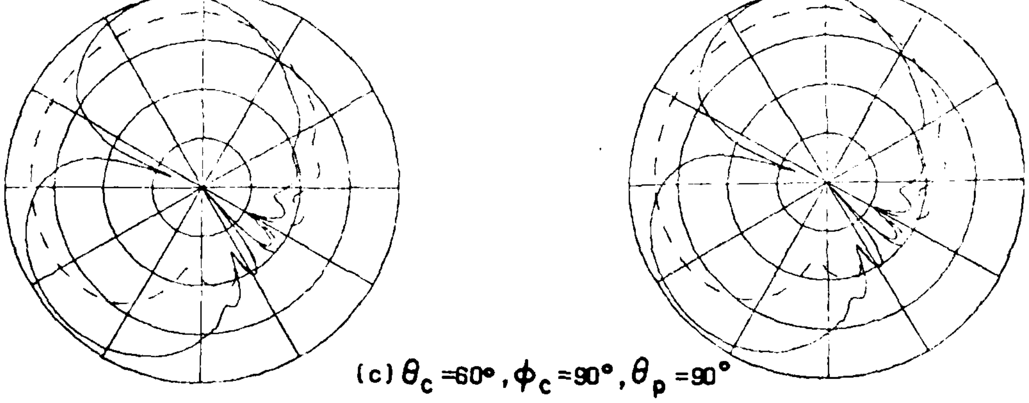

(c) $\theta_c = 60°$, $\phi_c = 90°$, $\theta_p = 90°$

Figure 11. Comparison of radiation patterns for a short monopole mounted at $\phi_s = 30°$, $\theta_s = 120°$ on a $2\lambda \times 10\lambda$ spheriod.

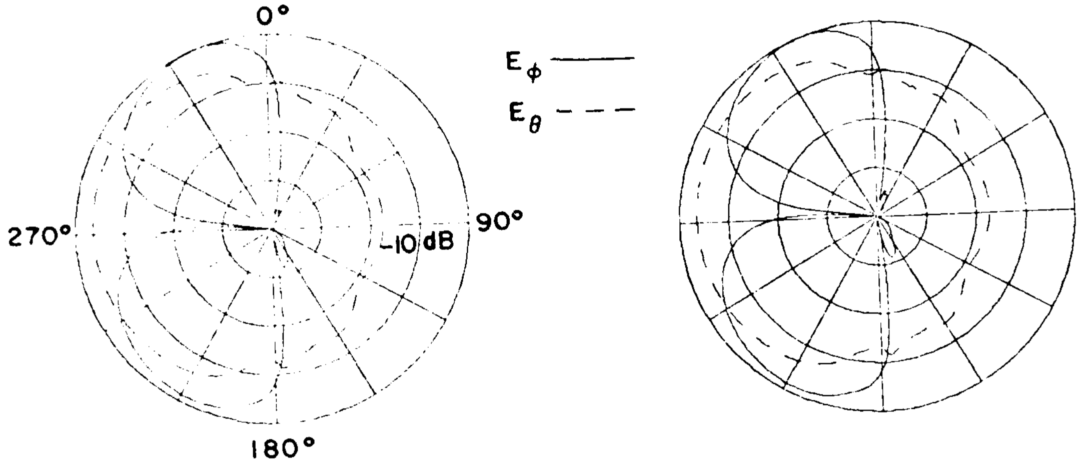

(d) $\theta_c = 90°$, $\phi_c = 90°$, $\theta_p = 90°$

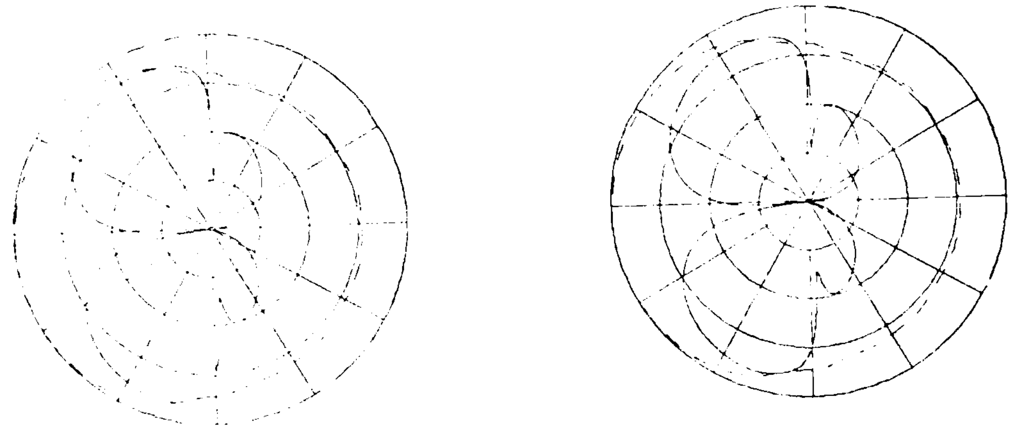

(e) $\theta_c = 90°$, $\phi_c = 0°$, $\theta_p = 90°$

Ellipsoid Program

Spheroid Program

Figure 11. (continued)

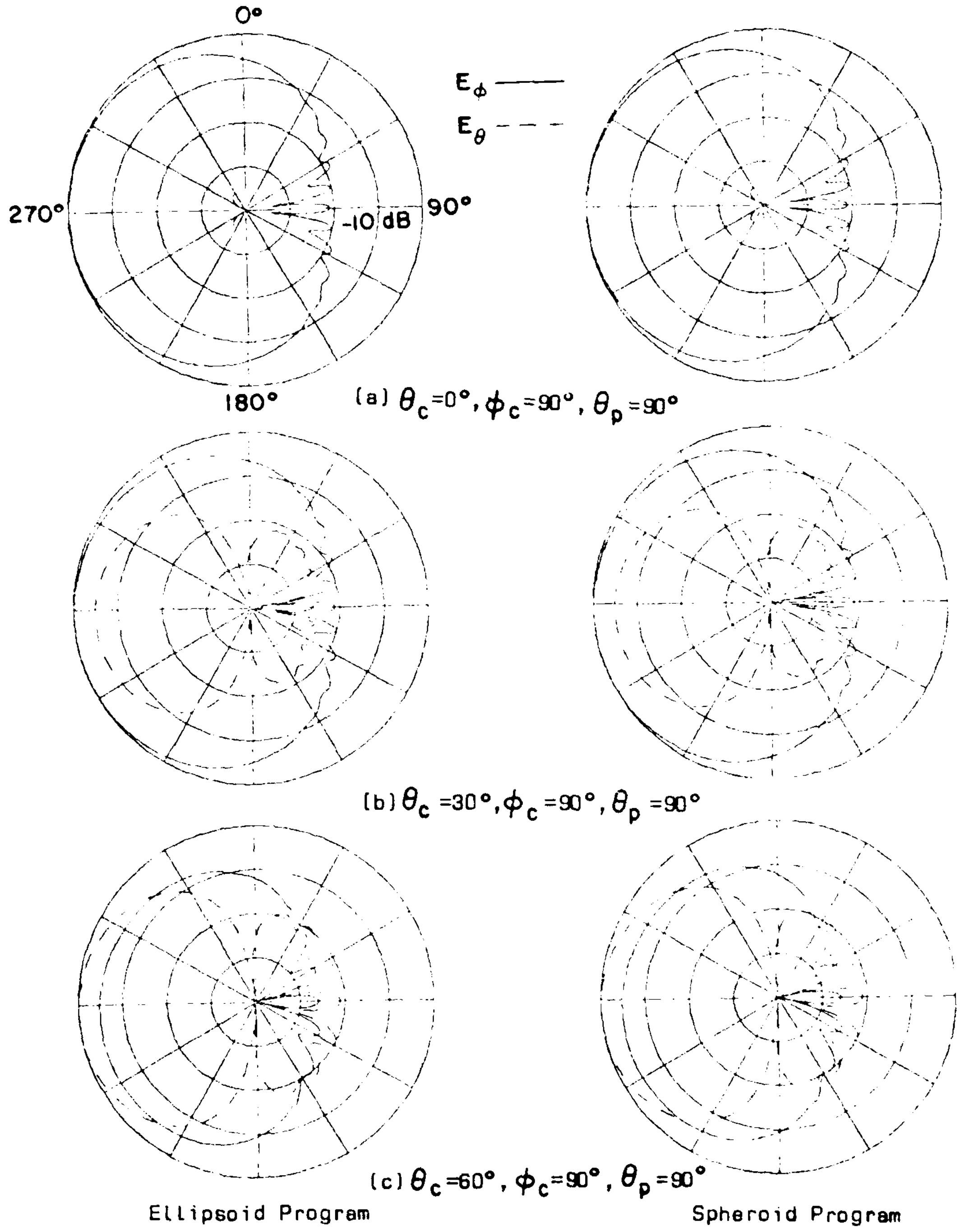

(a) $\theta_c = 0°$, $\phi_c = 90°$, $\theta_p = 90°$

(b) $\theta_c = 30°$, $\phi_c = 90°$, $\theta_p = 90°$

(c) $\theta_c = 60°$, $\phi_c = 90°$, $\theta_p = 90°$

Figure 12. Comparison of radiation patterns for an axial slot mounted at $\phi_s = 0°$, $\theta_s = 60°$ on a 2λ x 10λ spheriod.

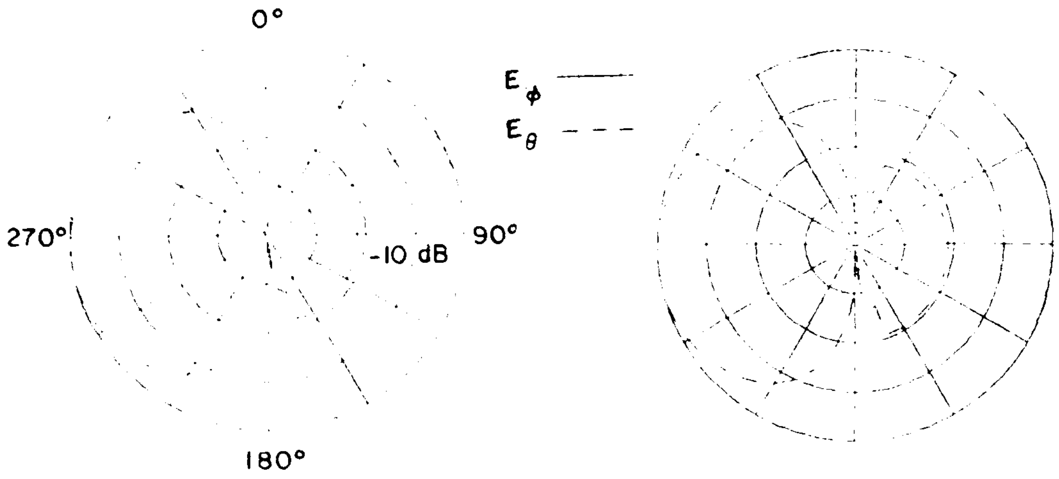

(d) $\theta_c = 90°, \phi_c = 90°, \theta_p = 90°$

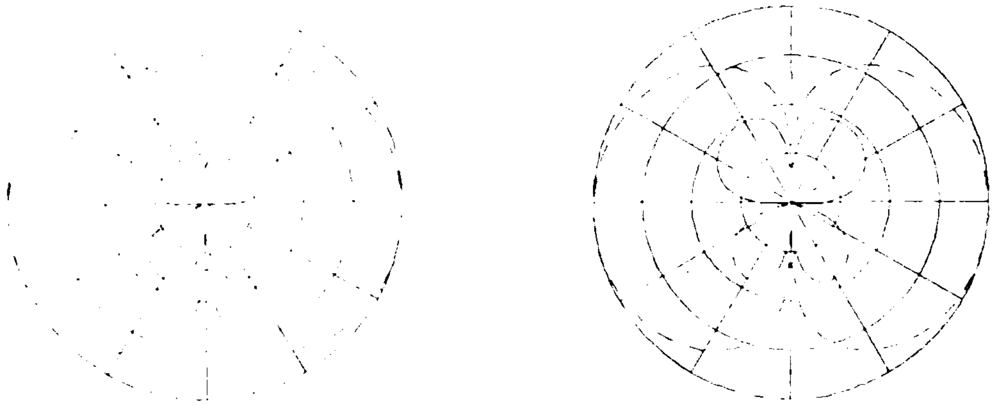

(e) $\theta_c = 90°, \phi_c = 0°, \theta_p = 90°$

Ellipsoid Program

Spheroid Program

Figure 12. (continued)

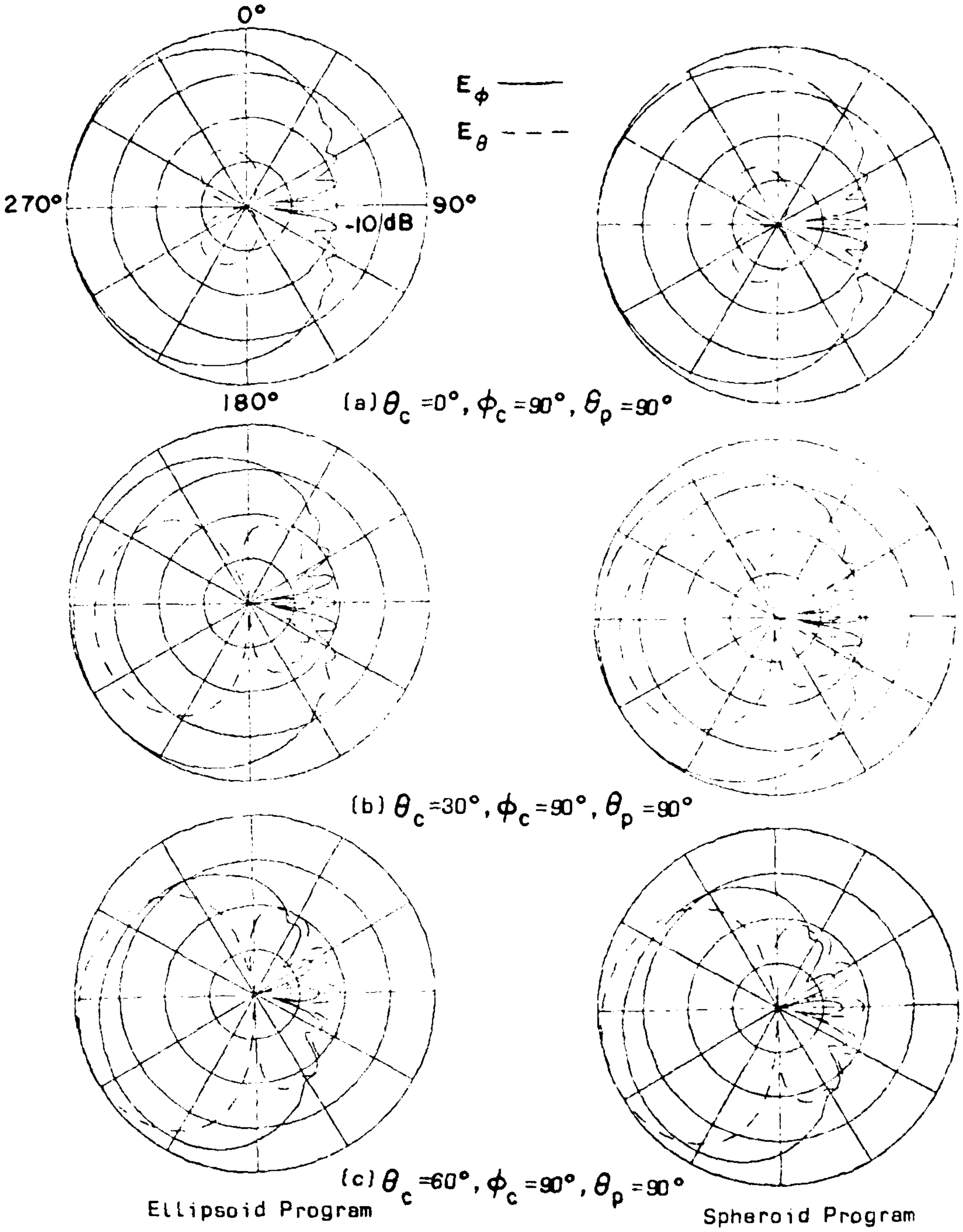

(a) θ_c =0°, ϕ_c =90°, θ_p =90°

(b) θ_c=30°, ϕ_c =90°, θ_p =90°

(c) θ_c =60°, ϕ_c =90°, θ_p =90°

Ellipsoid Program

Spheroid Program

Figure 13. Comparison of radiation patterns for an axial slot mounted at ϕ_s = 0°, θ_s = 30° on a 2λ x 10λ spheriod.

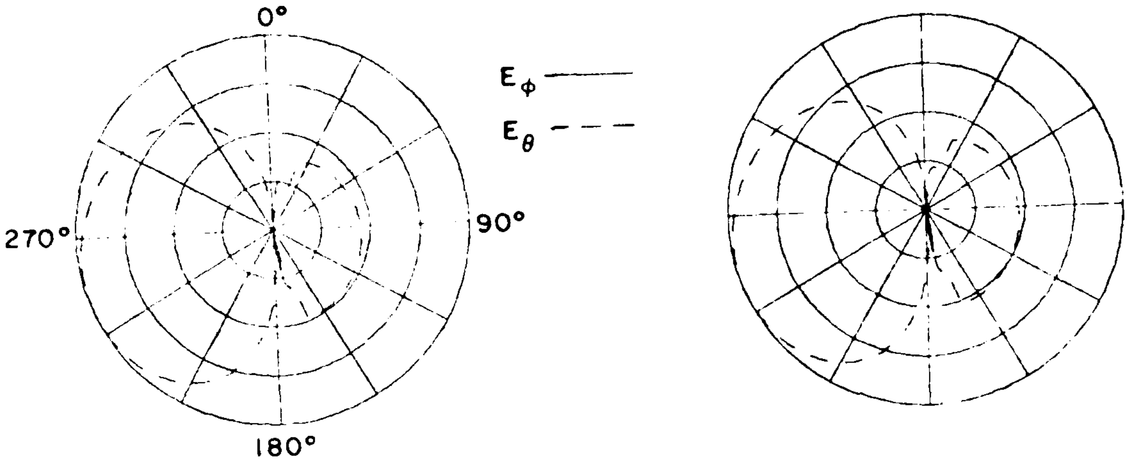

(d) $\theta_c = 90°$, $\phi_c = 90°$, $\theta_p = 90°$

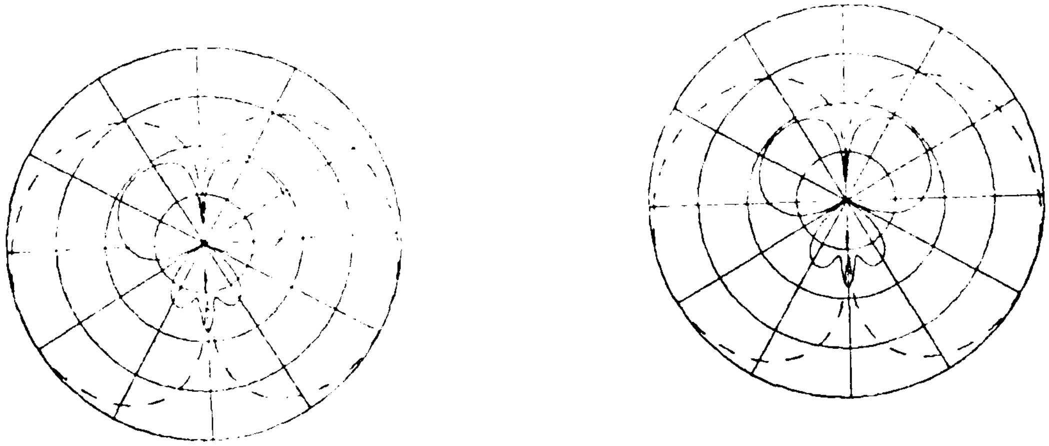

(e) $\theta_c = 90°$, $\phi_c = 0°$, $\theta_p = 90°$

Ellipsoid Program

Spheroid Program

Figure 13. (continued)

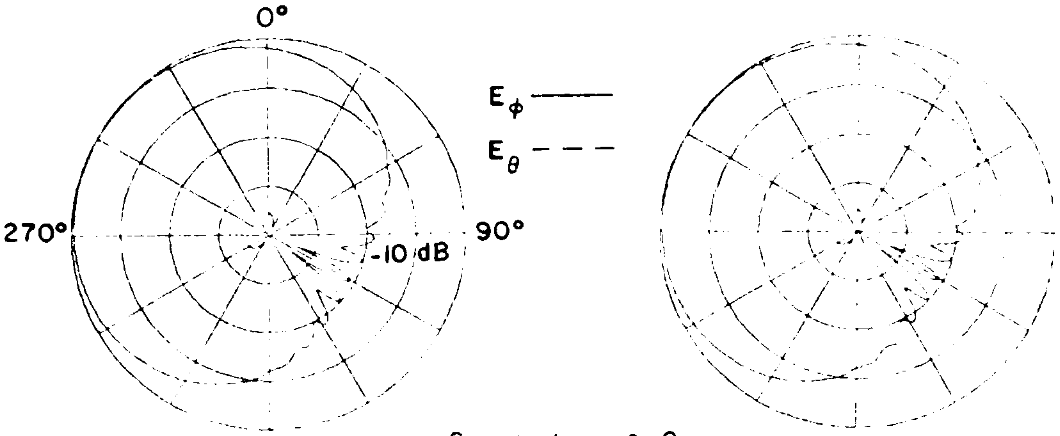

(a) θ_c=0°, ϕ_c=90°, θ_p=90°

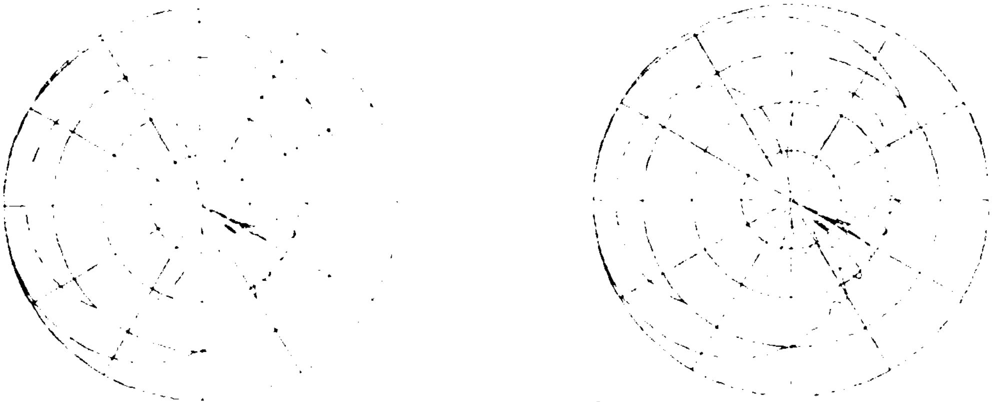

(b) θ_c =30°, ϕ_c =90°, θ_p =90°

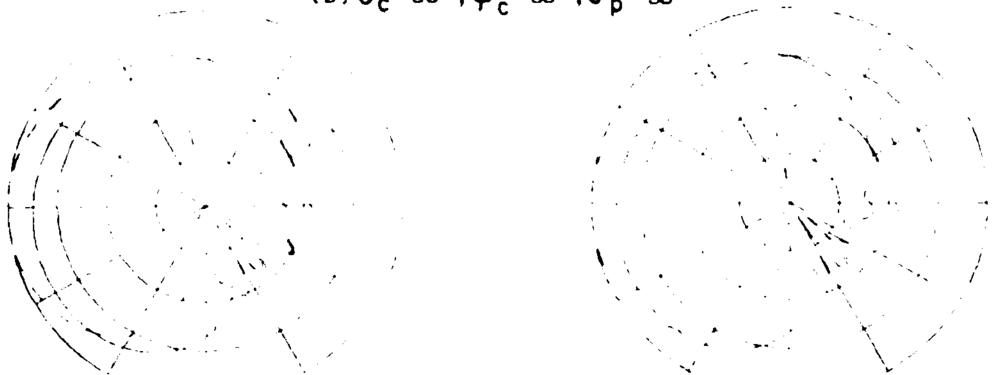

(c) θ_c =60°, ϕ_c =90°, θ_p =90°

Ellipsoid Program

Spheroid Program

Figure 14. Comparison of radiation patterns for an axial slot mounted at θ_s = 30°, ϕ_s = 60° on a 2λ x 10λ spheriod.

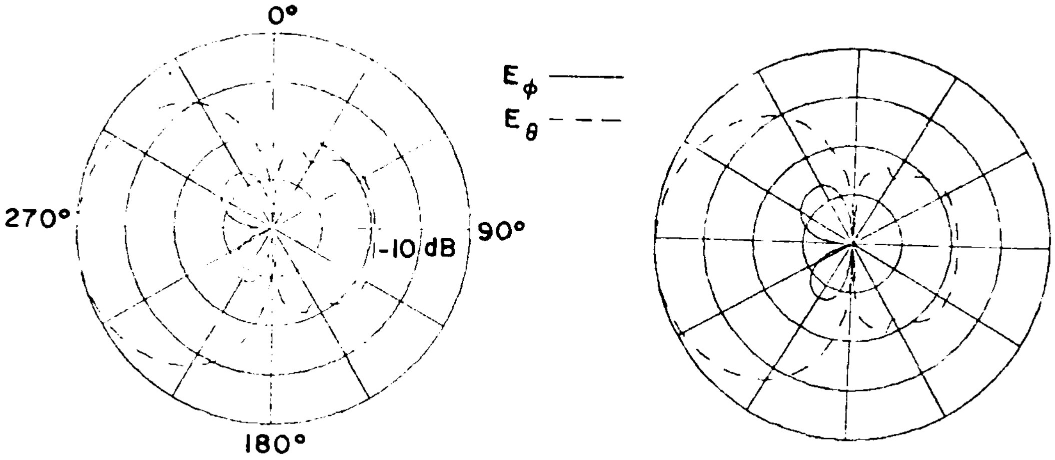

(d) $\theta_c = 90°, \phi_c = 90°, \theta_p = 90°$

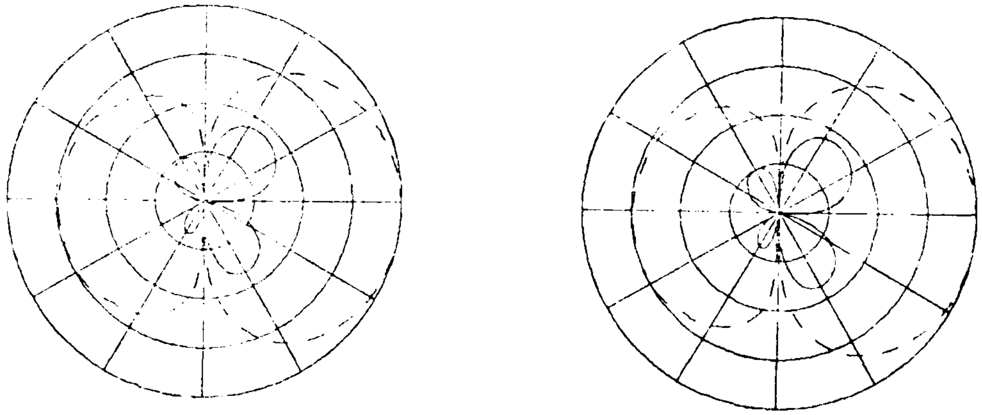

(e) $\theta_c = 90°, \phi_c = 0°, \theta_p = 90°$

Ellipsoid Program

Spheroid Program

Figure 14. (continued)

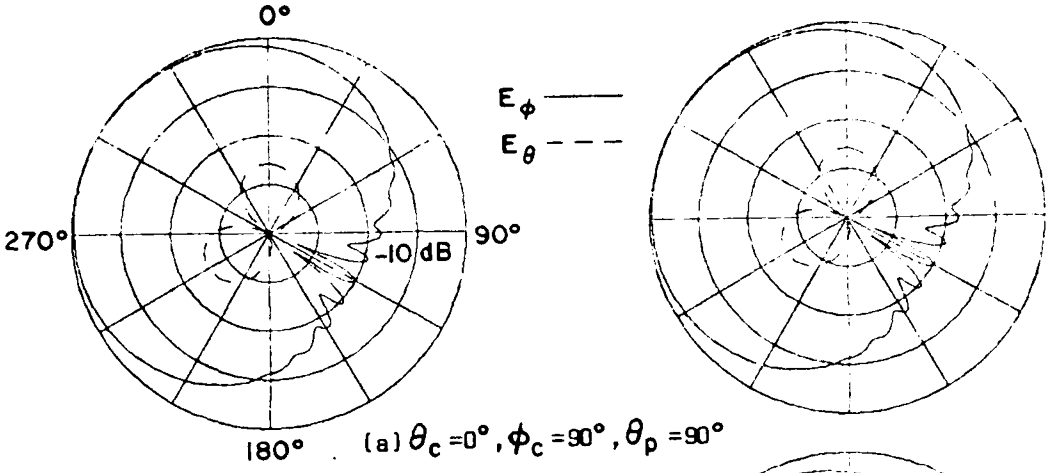

(a) $\theta_c = 0°, \phi_c = 90°, \theta_p = 90°$

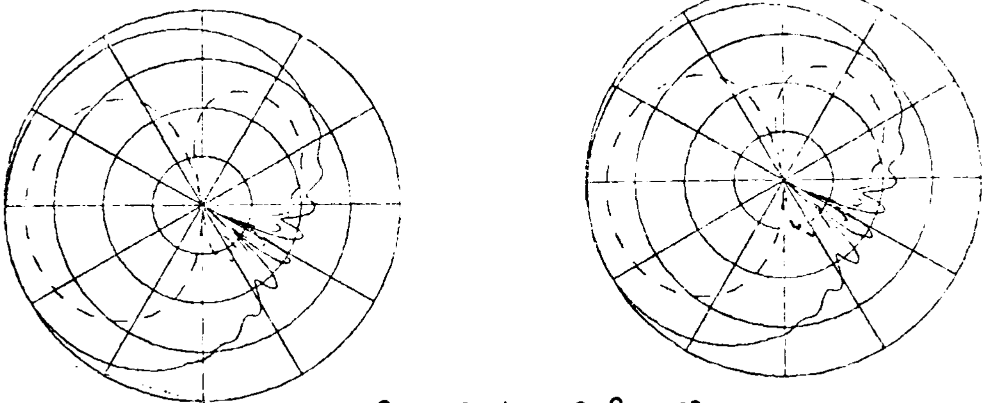

(b) $\theta_c = 30°, \phi_c = 90°, \theta_p = 90°$

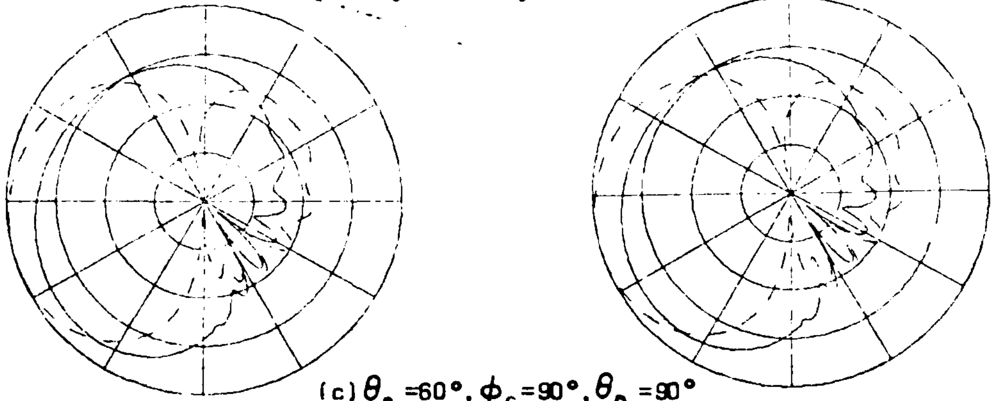

(c) $\theta_c = 60°, \phi_c = 90°, \theta_p = 90°$

Ellipsoid Program

Spheroid Program

Figure 15. Comparison of radiation patterns for an axial slot mounted at ϕ_s = 30°, θ_s = 30° on a 2λ x 10λ spheriod.

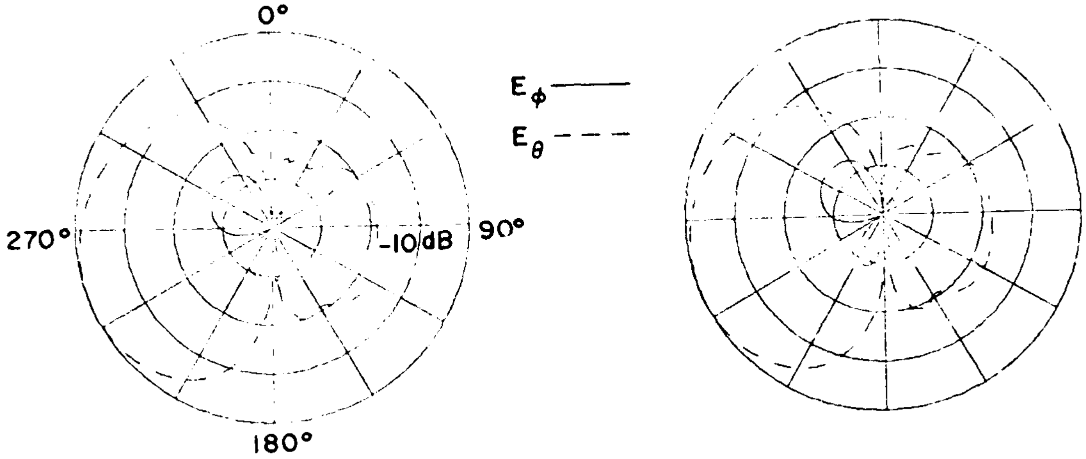

(d) $\theta_c = 90°$, $\phi_c = 90°$, $\theta_p = 90°$

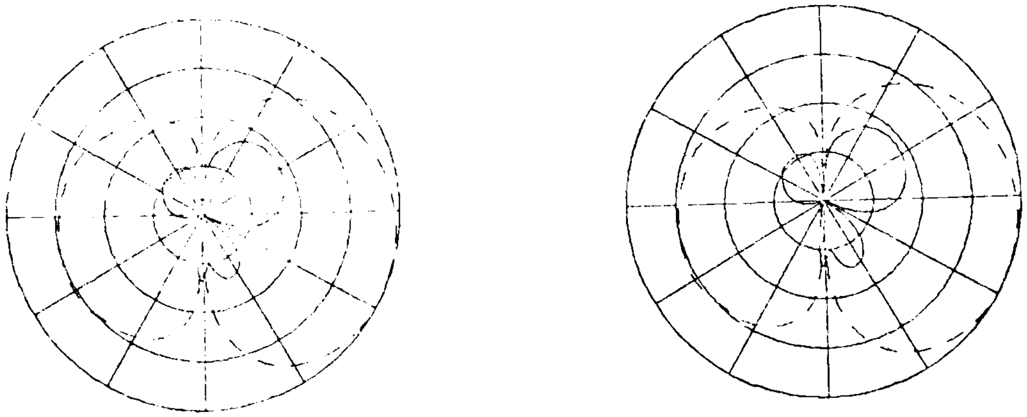

(e) $\theta_c = 90°$, $\phi_c = 0°$, $\theta_p = 90°$

Ellipsoid Program

Spheroid Program

Figure 15. (continued)

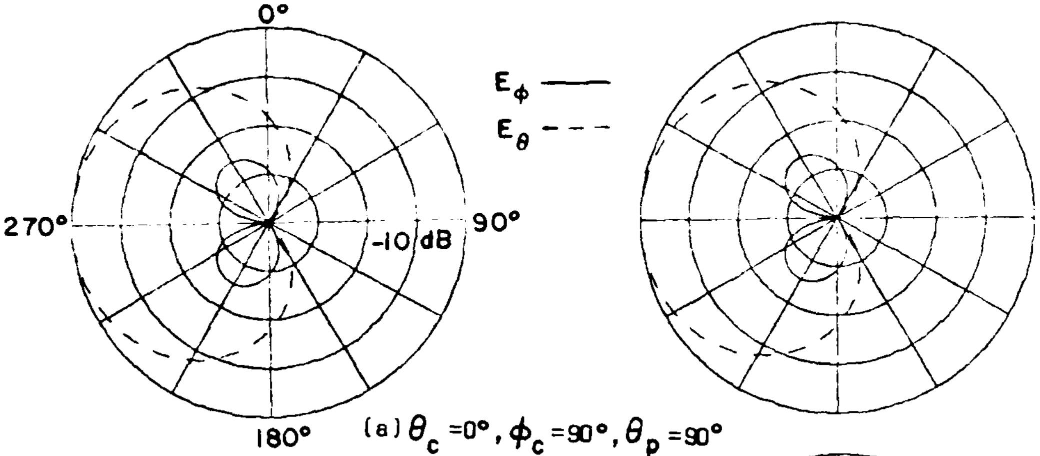

(a) θ_c =0°, ϕ_c =90°, θ_p =90°

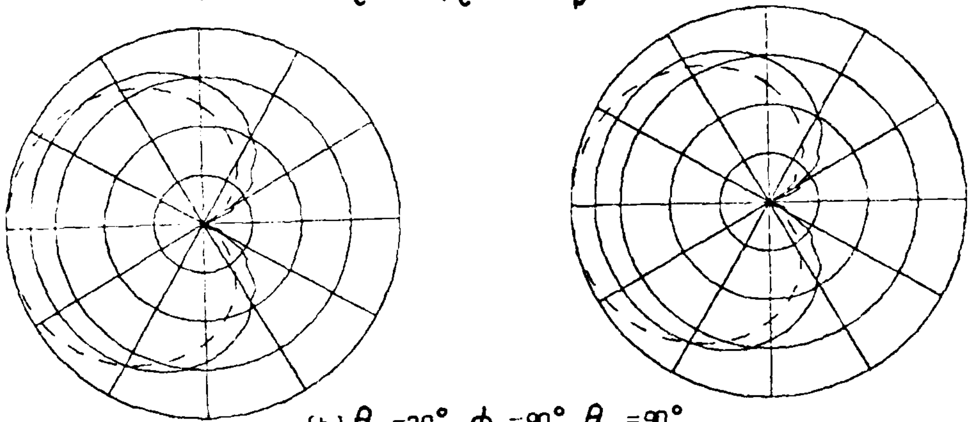

(b) θ_c =30°, ϕ_c=90°, θ_p =90°

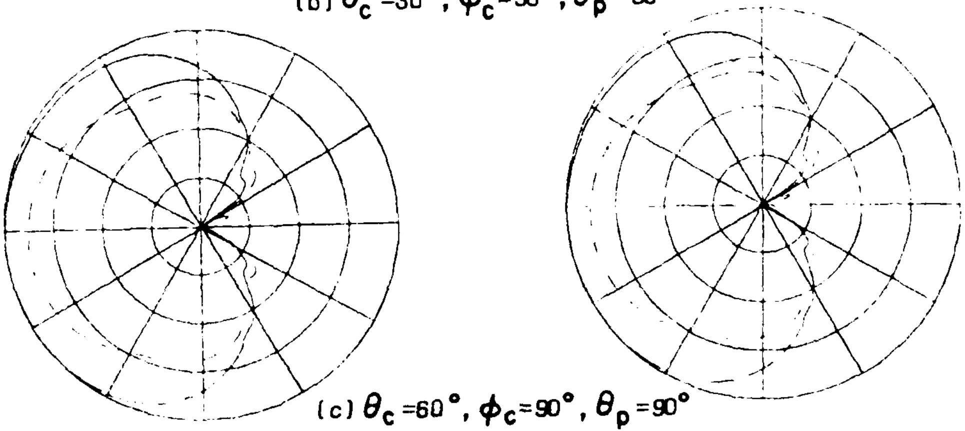

(c) θ_c =60°, ϕ_c=90°, θ_p =90°

Figure 16. Comparison of radiation patterns for a circumferential slot mounted at ϕ_s = 0°, θ_s = 60° on a 2λ x 10λ spheriod.

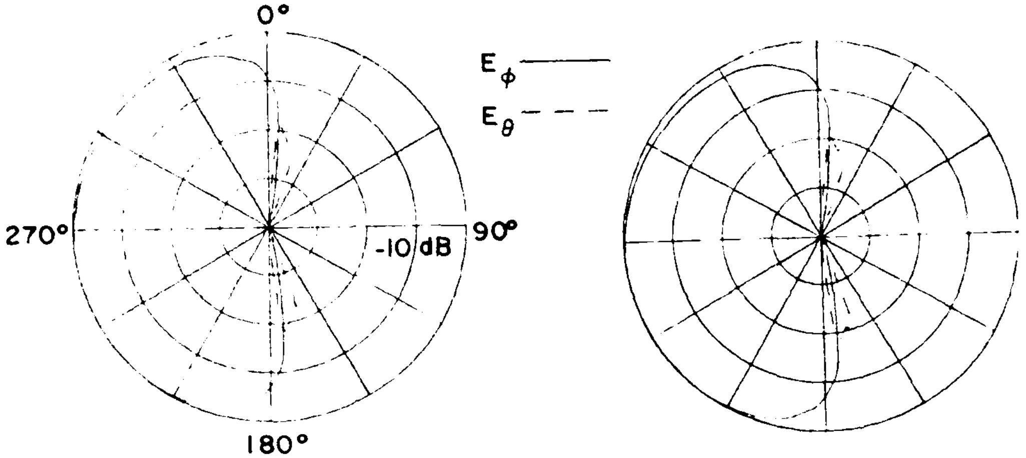

(d) $\theta_c = 90°$, $\phi_c = 90°$, $\theta_p = 90°$

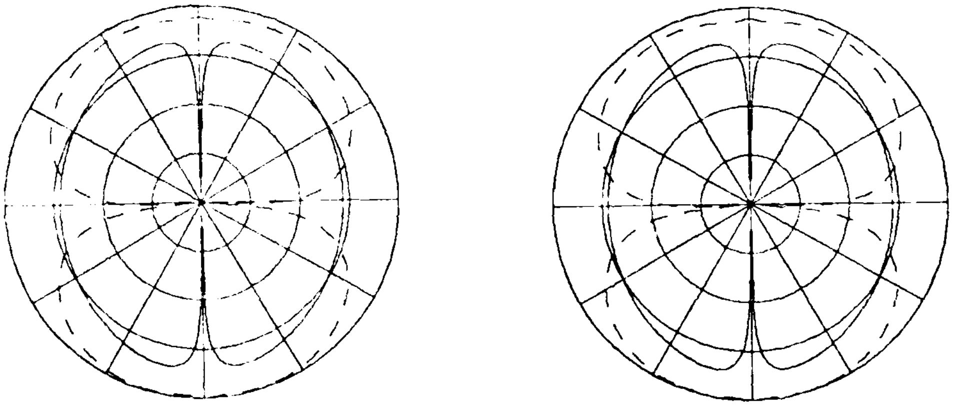

(e) $\theta_c = 90°$, $\phi_c = 0°$, $\theta_p = 90°$

Ellipsoid Program

Spheroid Program

Figure 16. (continued)

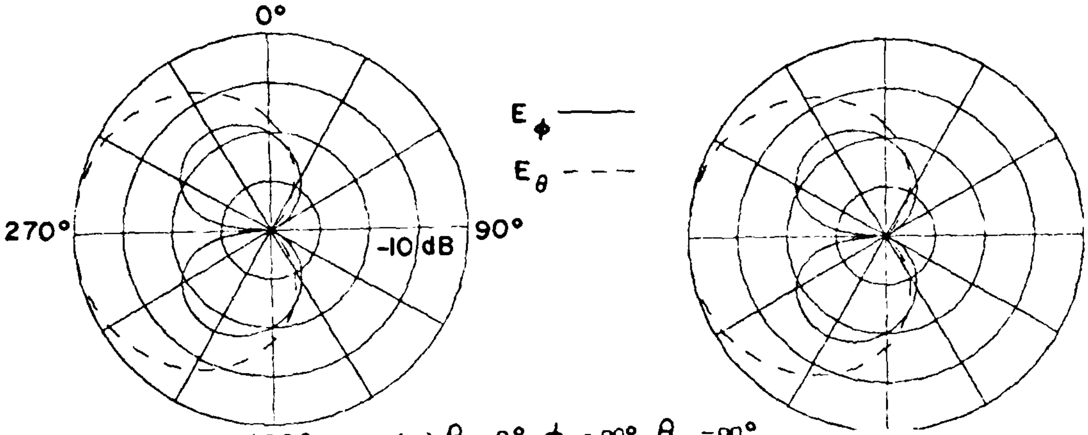

(a) $\theta_c = 0°$, $\phi_c = 90°$, $\theta_p = 90°$

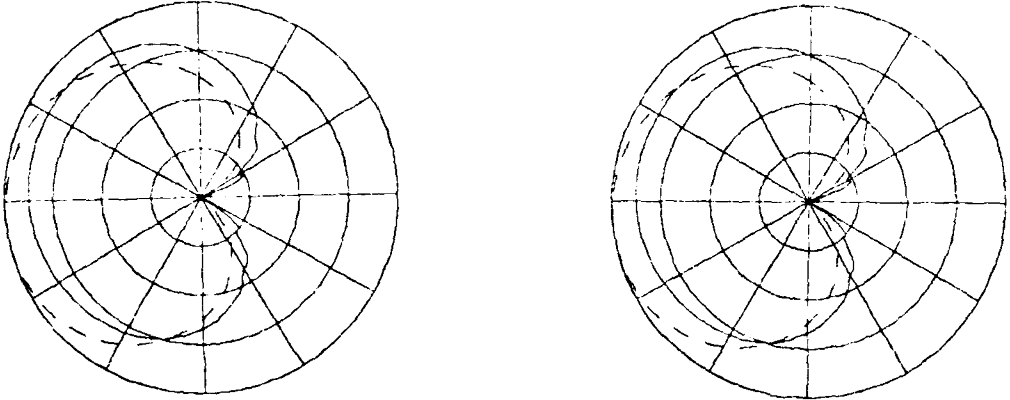

(b) $\theta_c = 30°$, $\phi_c = 90°$, $\theta_p = 90°$

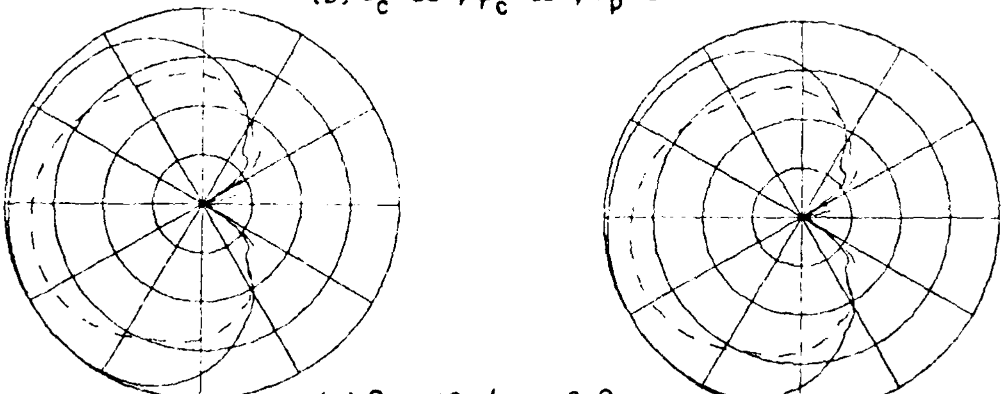

(c) $\theta_c = 60°$, $\phi_c = 90°$, $\theta_p = 90°$

Ellipsoid Program

Spheroid Program

Figure 17. Comparison of radiation patterns for a circumferential slot mounted at $\phi_s = 0°$, $\theta_s = 30°$ on a $2\lambda \times 10\lambda$ spheriod.

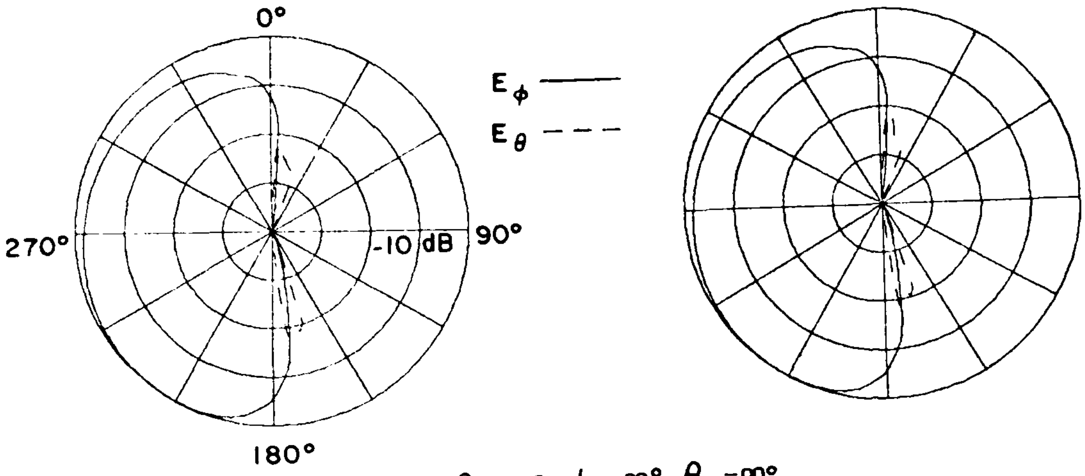

(d) $\theta_c = 90°$, $\phi_c = 90°$, $\theta_p = 90°$

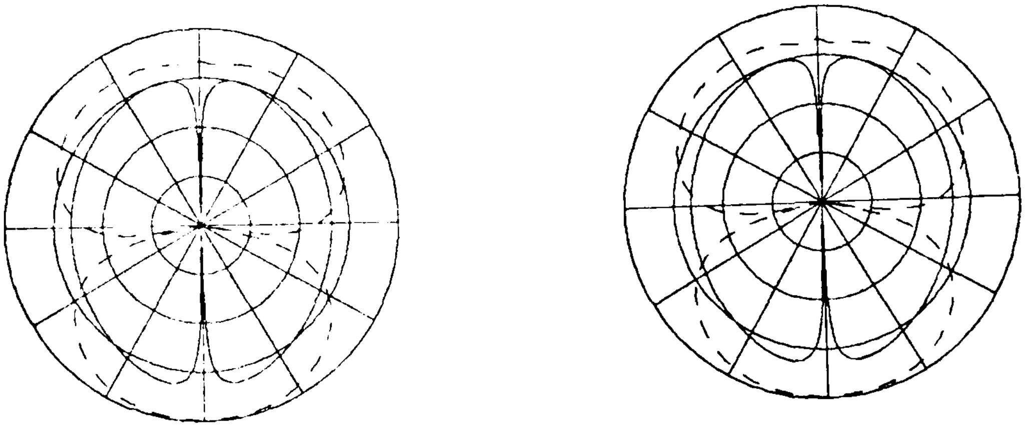

(e) $\theta_c = 90°$, $\phi_c = 0°$, $\theta_p = 90°$

Ellipsoid Program

Spheroid Program

Figure 17. (continued)

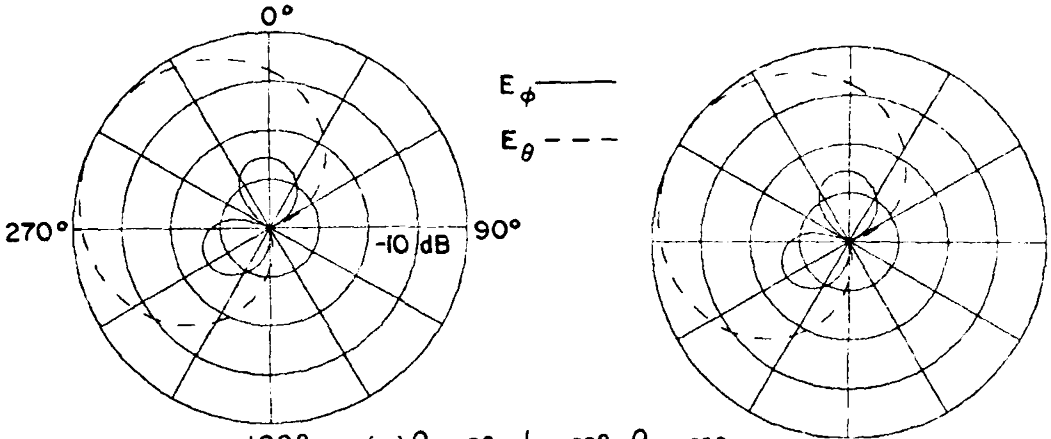

(a) θ_c =0°, ϕ_c=90°, θ_p =90°

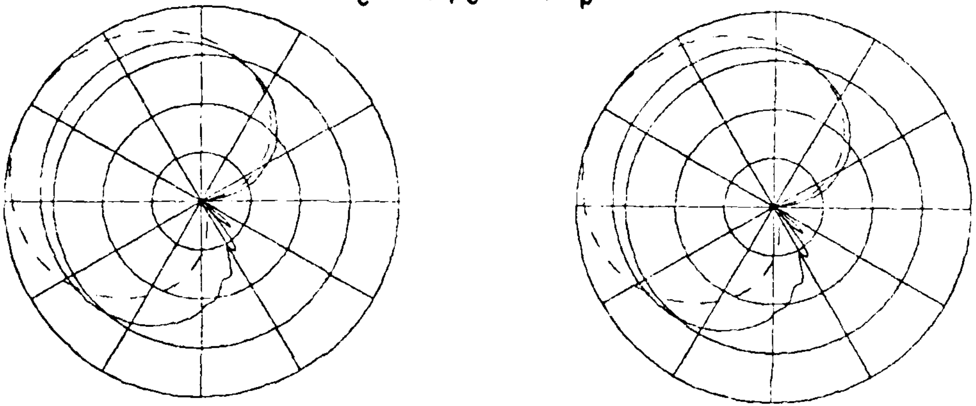

(b) θ_c=30°, ϕ_c =90°, θ_p =90°

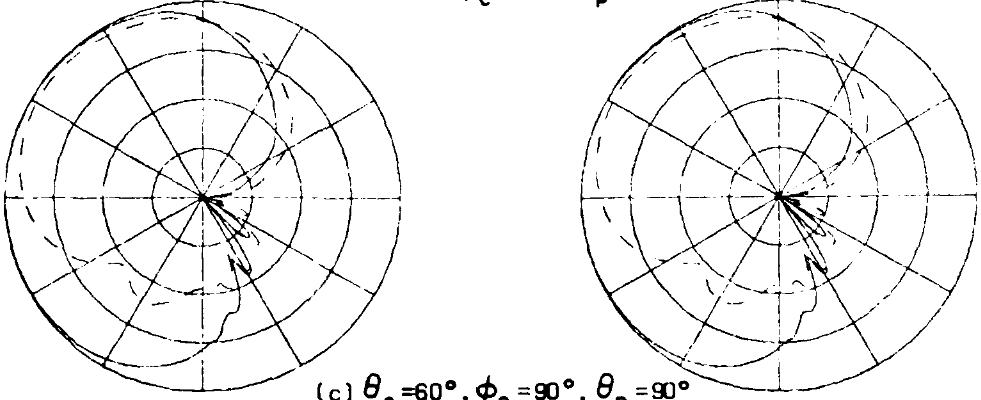

(c) θ_c =60°, ϕ_c =90°, θ_p =90°

Figure 18. Comparison of radiation patterns for a circumferential slot mounted at ϕ_s = 30°, θ_s = 60° on a 2λ x 10λ spheriod.

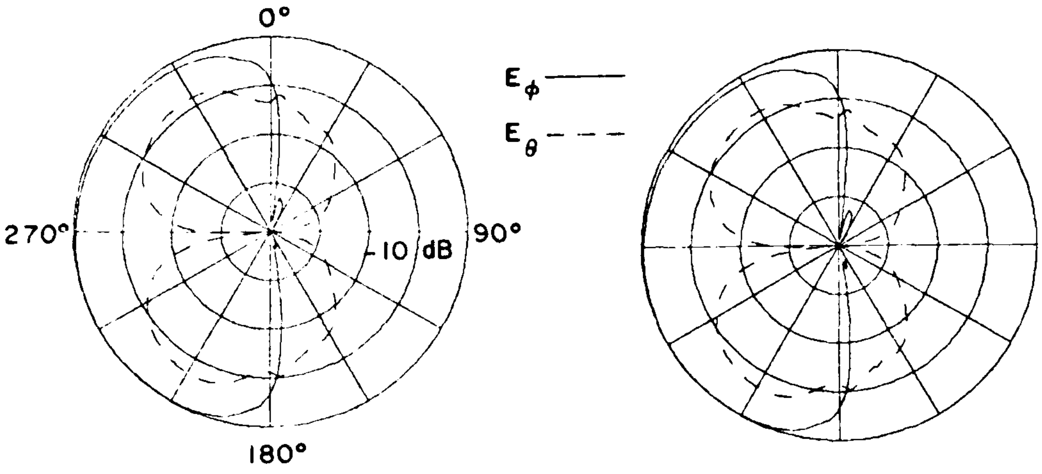

(d) $\theta_c = 90°, \phi_c = 90°, \theta_p = 90°$

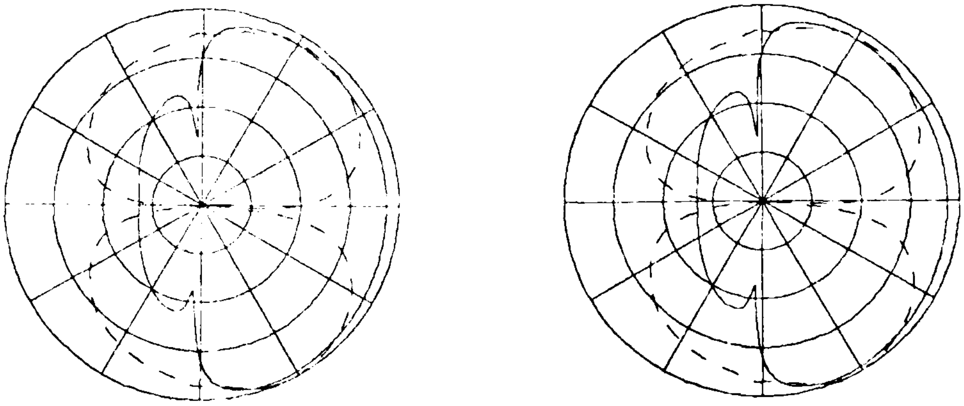

(e) $\theta_c = 90°, \phi_c = 0°, \theta_p = 90°$

Figure 18. (continued)

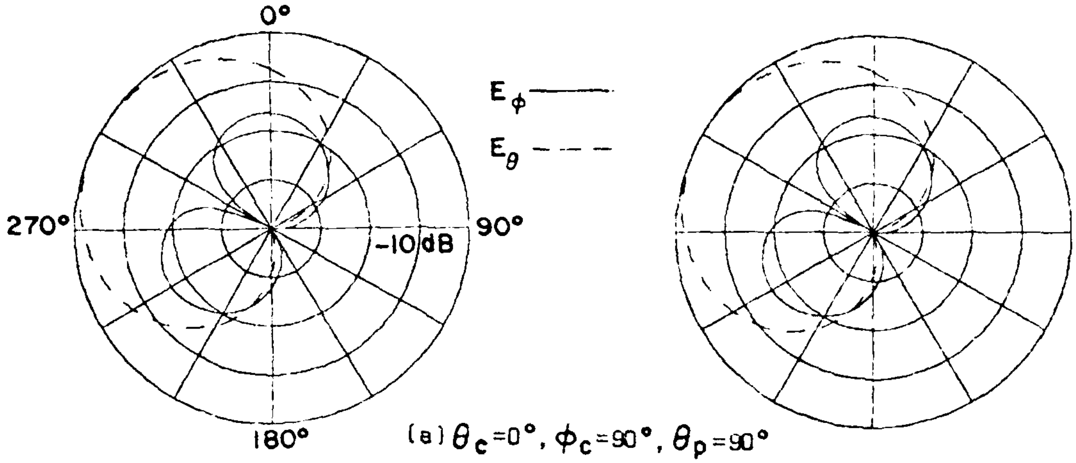

(a) $\theta_c=0°$, $\phi_c=90°$, $\theta_p=90°$

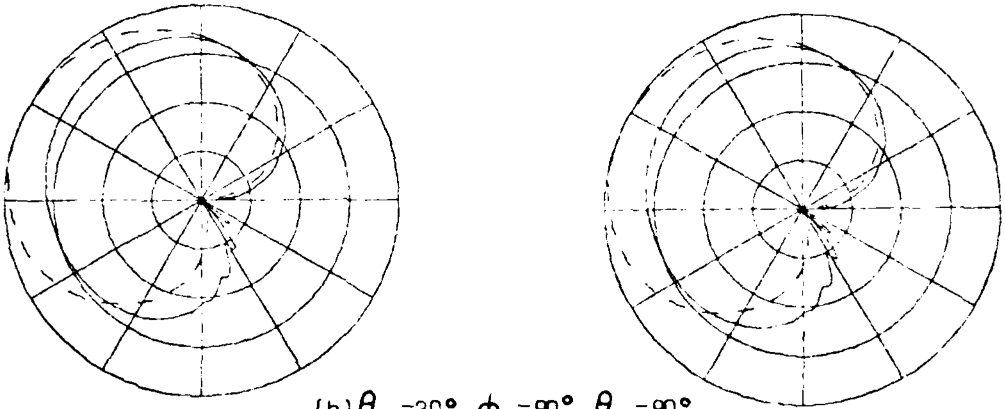

(b) $\theta_c=30°$, $\phi_c=90°$, $\theta_p=90°$

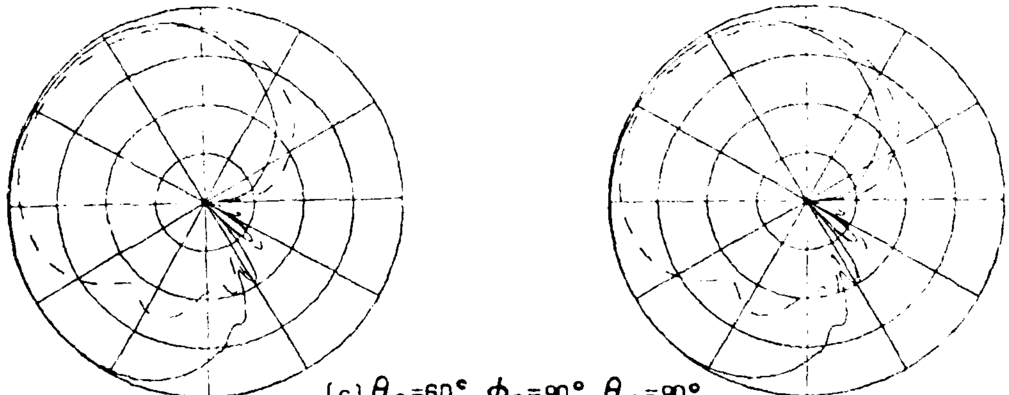

(c) $\theta_c=60°$, $\phi_c=90°$, $\theta_p=90°$

Ellipsoid Program

Spheroid Program

Figure 19. Comparison of radiation patterns for a circumferential slot mounted at $\phi_s = 30°$, $\theta_s = 30°$ on a $2\lambda \times 10\lambda$ spheroid.

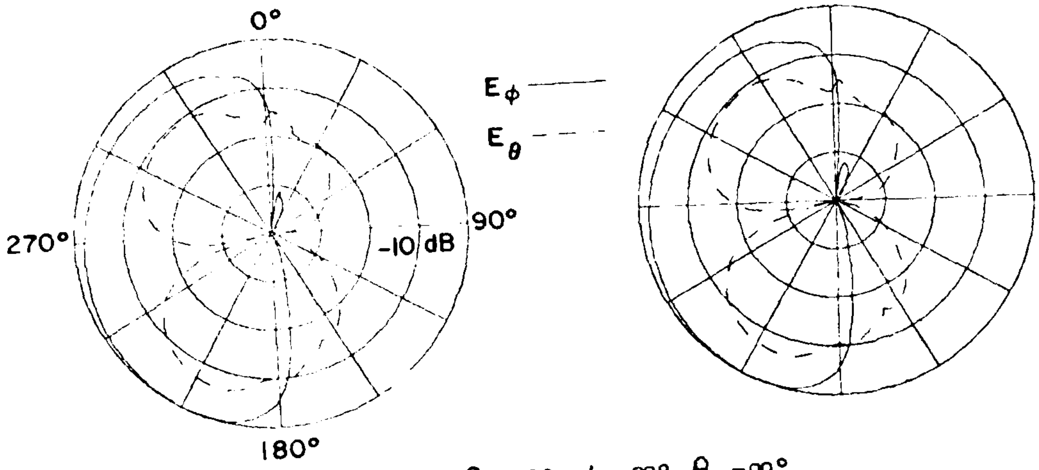

(d) $\theta_c=90°$, $\phi_c=90°$, $\theta_p=90°$

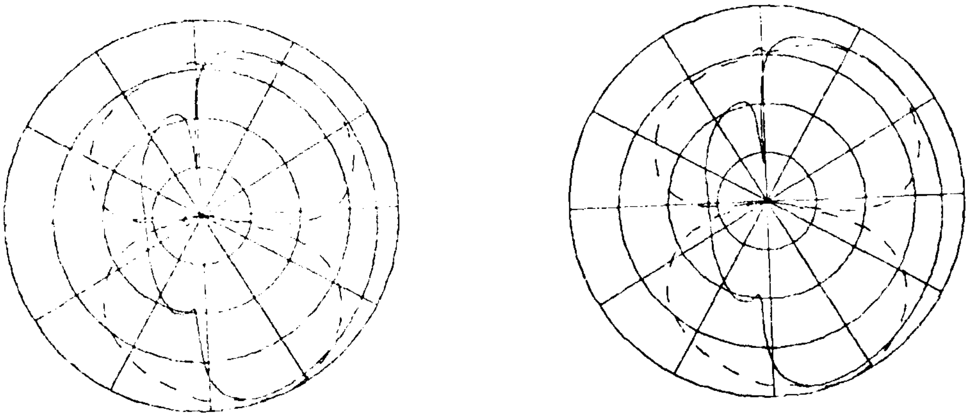

(e) $\theta_c=90°$, $\phi_c=0°$, $\theta_p=90°$

Ellipsoid Program

Spheroid Program

Figure 19. (continued)

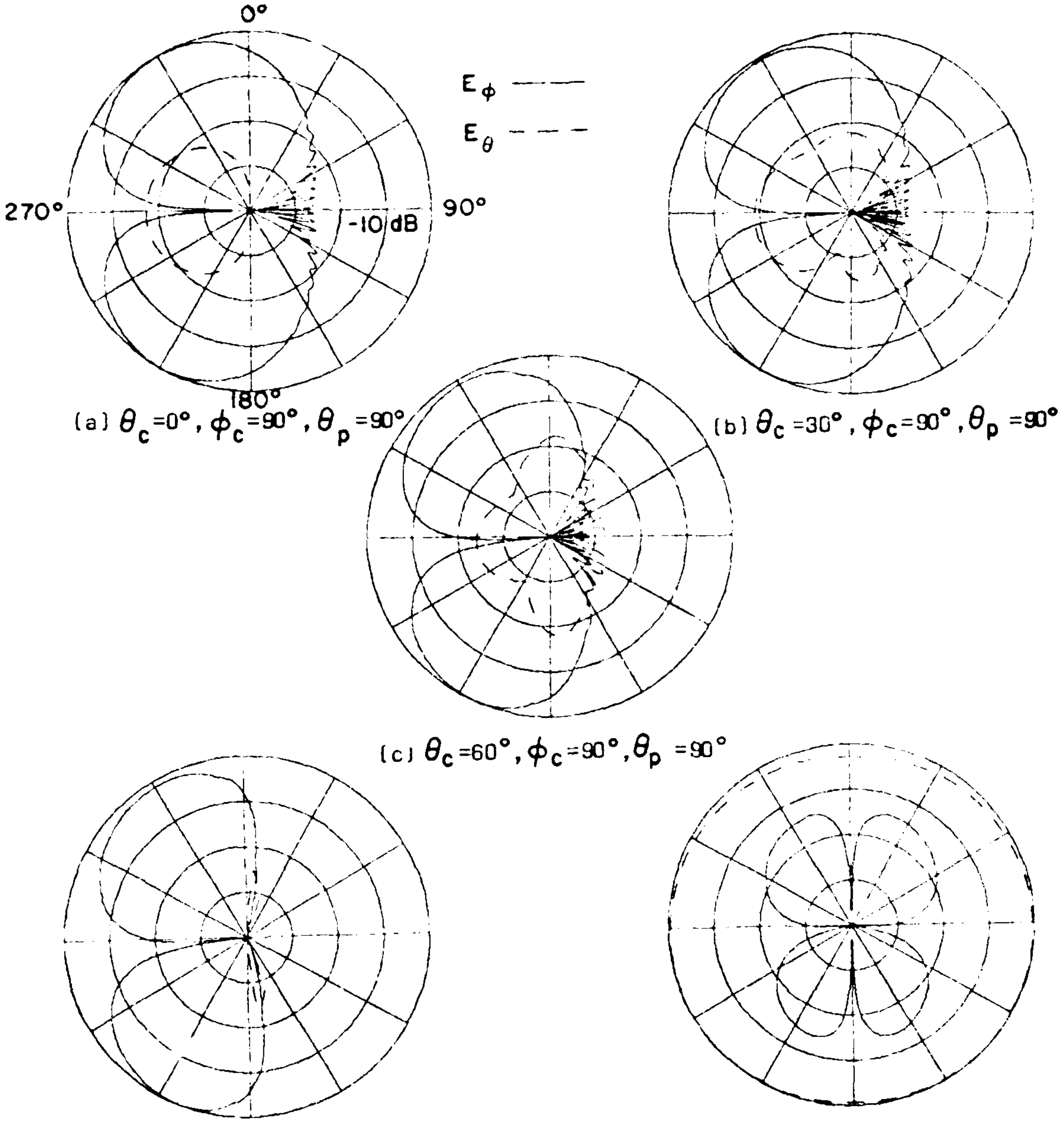

(a) θ_c = 0°, ϕ_c = 90°, θ_p = 90°

(b) θ_c = 30°, ϕ_c = 90°, θ_p = 90°

(c) θ_c = 60°, ϕ_c = 90°, θ_p = 90°

(d) θ_c = 90°, ϕ_c = 90°, θ_p = 90°

(e) θ_c = 90°, ϕ_c = 0°, θ_p = 90°

Figure 20. Radiation patterns for R_t = 15λ for a short monopole mounted at ϕ_s = 0°, θ_s = 60° on a 2λ x 4λ x 10λ ellipsoid.

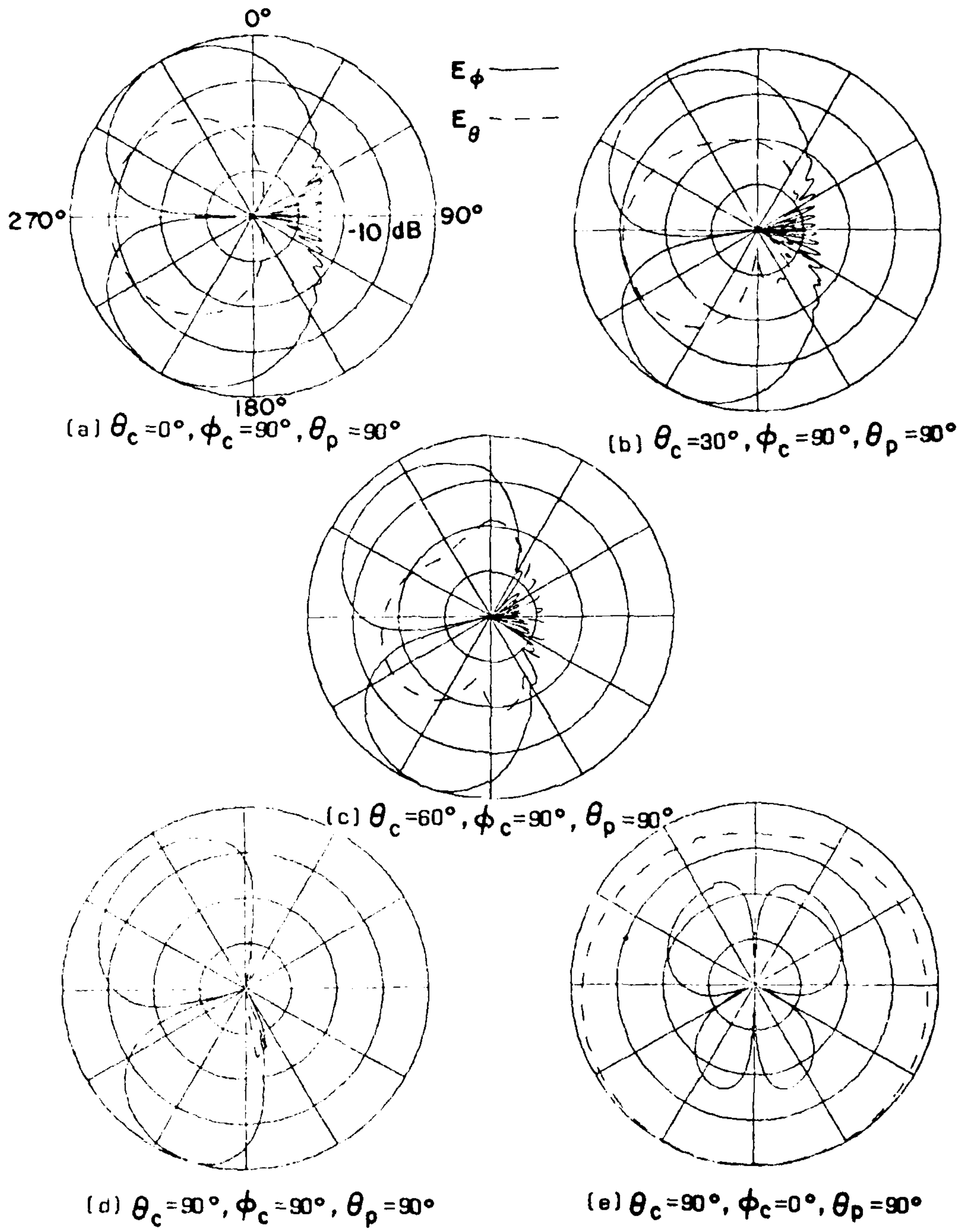

(a) $\theta_c = 0°, \phi_c = 90°, \theta_p = 90°$

(b) $\theta_c = 30°, \phi_c = 90°, \theta_p = 90°$

(c) $\theta_c = 60°, \phi_c = 90°, \theta_p = 90°$

(d) $\theta_c = 90°, \phi_c = 90°, \theta_p = 90°$

(e) $\theta_c = 90°, \phi_c = 0°, \theta_p = 90°$

Figure 21. Radiation patterns for a short monopole mounted at $\phi_s = 0°$, $\theta_s = 30°$ on a $2\lambda \times 4\lambda \times 10\lambda$ ellipsoid.

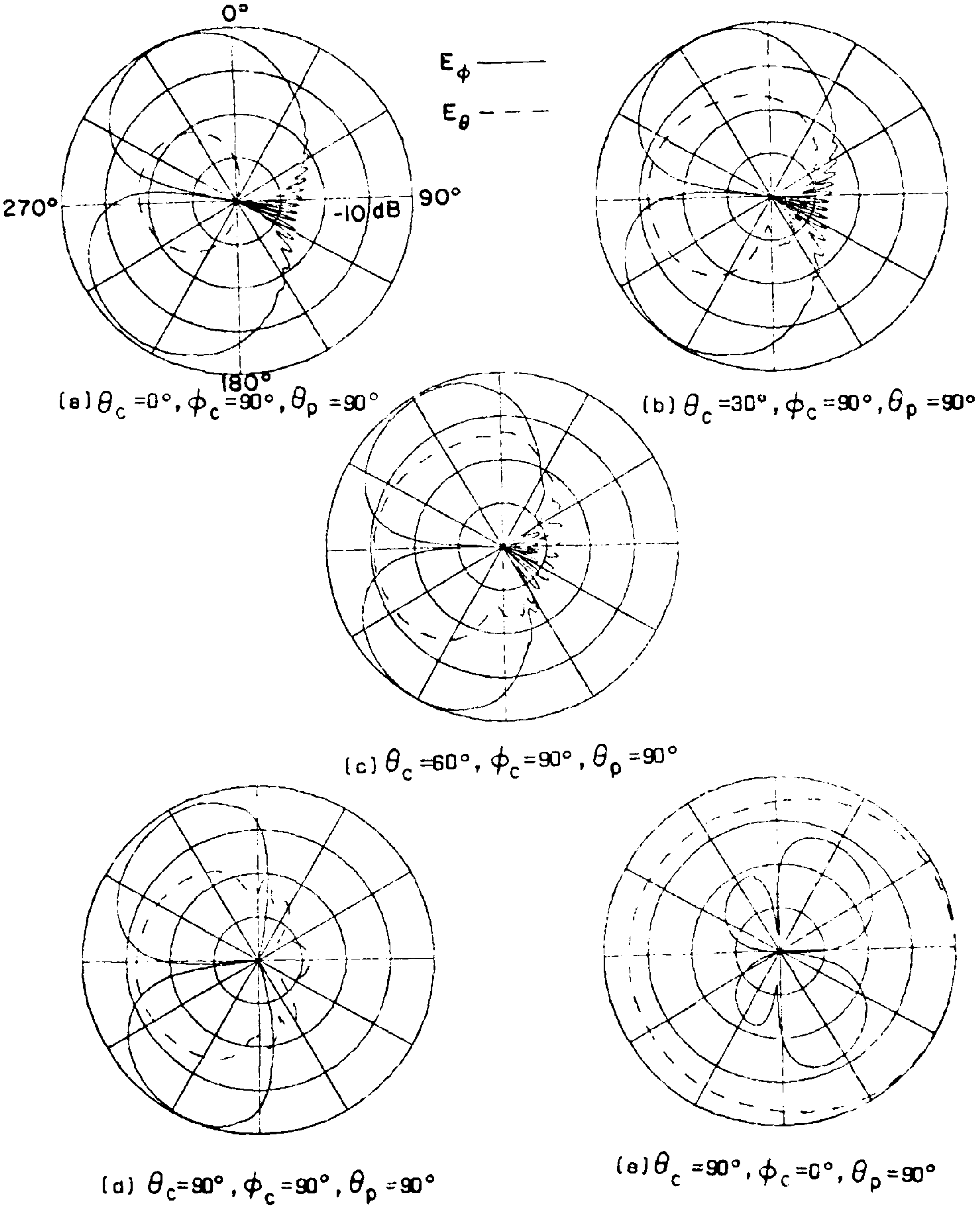

(a) $\theta_c = 0°, \phi_c = 90°, \theta_p = 90°$

(b) $\theta_c = 30°, \phi_c = 90°, \theta_p = 90°$

(c) $\theta_c = 60°, \phi_c = 90°, \theta_p = 90°$

(d) $\theta_c = 90°, \phi_c = 90°, \theta_p = 90°$

(e) $\theta_c = 90°, \phi_c = 0°, \theta_p = 90°$

Figure 22. Radiation patterns for a short monopole mounted at $\phi_s = 30°$, $\theta_s = 60°$ on a $2\lambda \times 4\lambda \times 10\lambda$ ellipsoid.

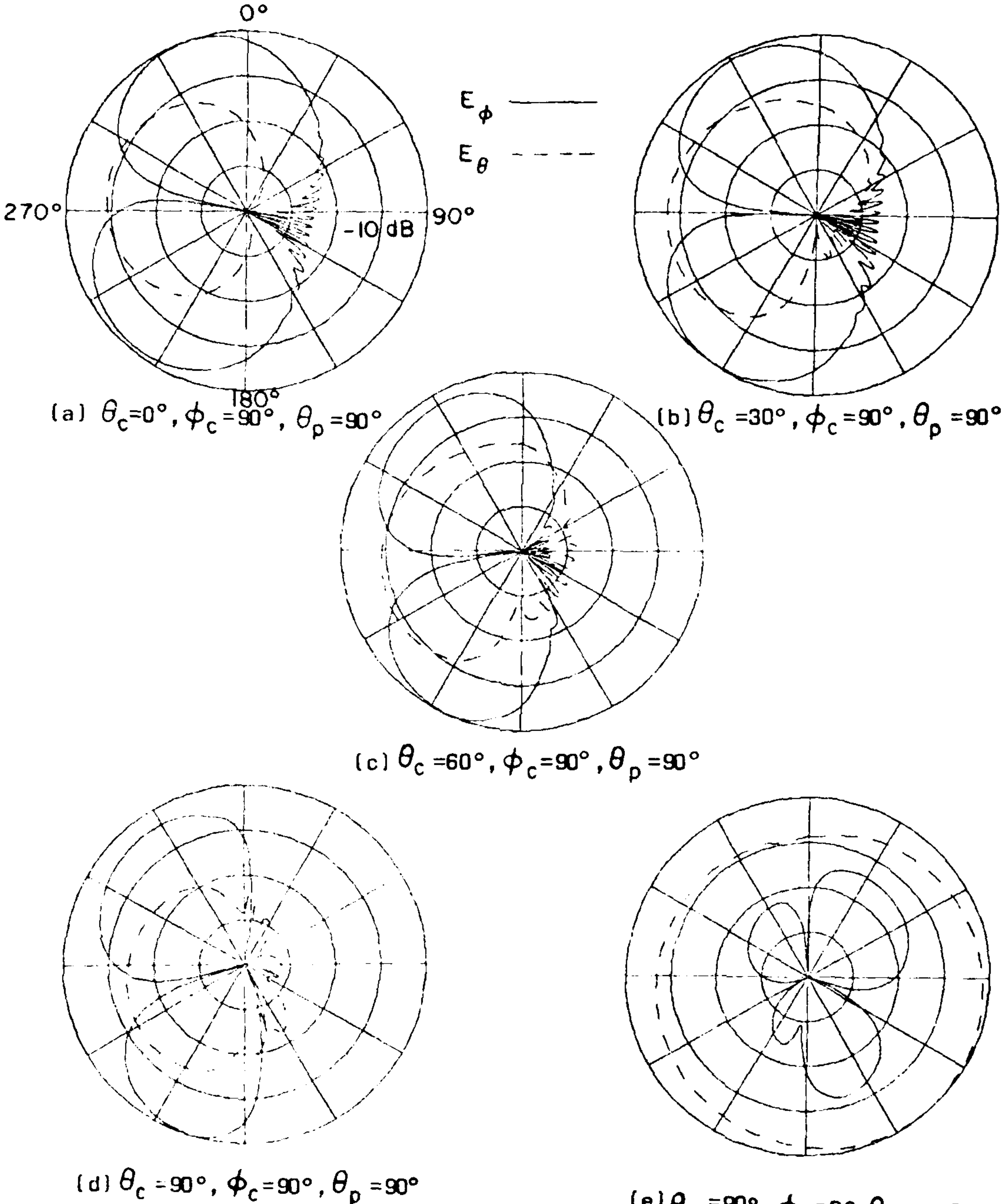

(a) $\theta_c=0°$, $\phi_c=90°$, $\theta_p=90°$

(b) $\theta_c=30°$, $\phi_c=90°$, $\theta_p=90°$

(c) $\theta_c=60°$, $\phi_c=90°$, $\theta_p=90°$

(d) $\theta_c=90°$, $\phi_c=90°$, $\theta_p=90°$

(e) $\theta_c=90°$, $\phi_c=0°$, $\theta_p=90°$

Figure 23. Radiation patterns for a short monopole mounted at $\phi_s = 30°$, $\theta_s = 30°$ on a 2λ x 4λ x 10λ ellipsoid.

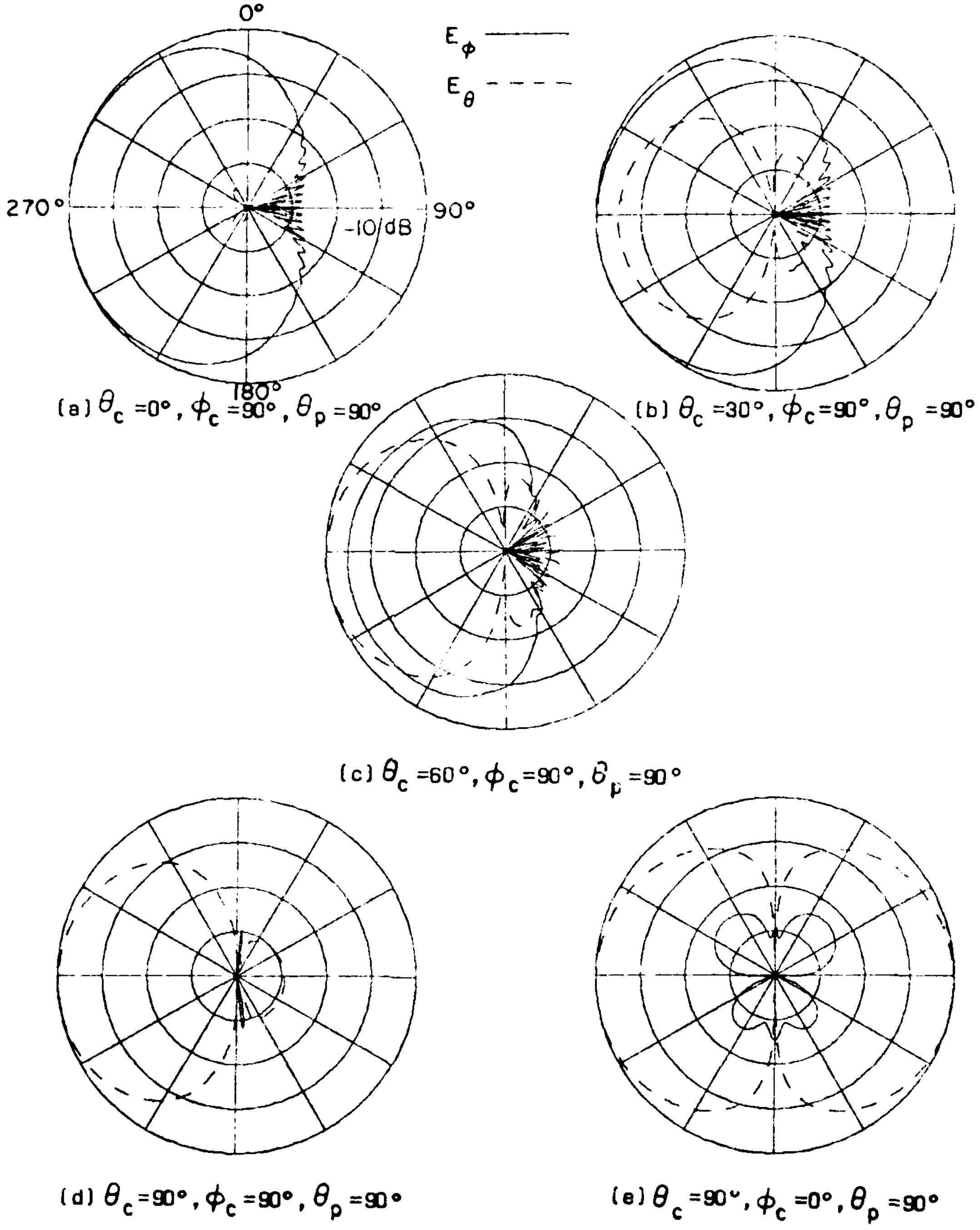

(a) $\theta_c = 0°$, $\phi_c = 90°$, $\theta_p = 90°$

(b) $\theta_c = 30°$, $\phi_c = 90°$, $\theta_p = 90°$

(c) $\theta_c = 60°$, $\phi_c = 90°$, $\theta_p = 90°$

(d) $\theta_c = 90°$, $\phi_c = 90°$, $\theta_p = 90°$

(e) $\theta_c = 90°$, $\phi_c = 0°$, $\theta_p = 90°$

Figure 24. Radiation patterns for an axial slot mounted at $\phi_s = 0°$, $\theta_s = 60°$ on a $2\lambda \times 4\lambda \times 10\lambda$ ellipsoid.

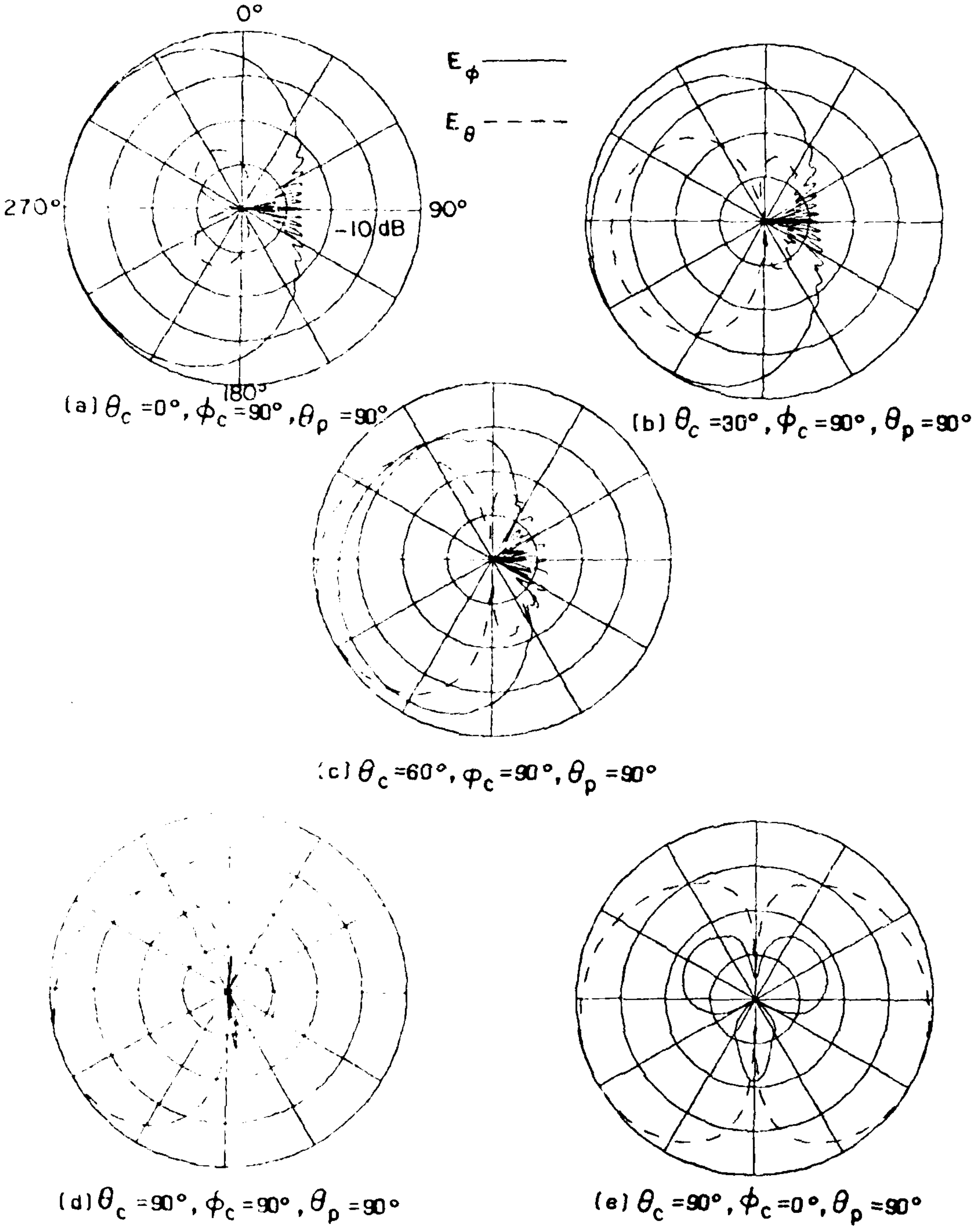

(a) $\theta_c = 0°, \phi_c = 90°, \theta_p = 90°$

(b) $\theta_c = 30°, \phi_c = 90°, \theta_p = 90°$

(c) $\theta_c = 60°, \phi_c = 90°, \theta_p = 90°$

(d) $\theta_c = 90°, \phi_c = 90°, \theta_p = 90°$

(e) $\theta_c = 90°, \phi_c = 0°, \theta_p = 90°$

Figure 25. Radiation patterns for an axial slot mounted at $\phi_s = 0°$, $\theta_s = 30°$ on a $2\lambda \times 4\lambda \times 10\lambda$ ellipsoid.

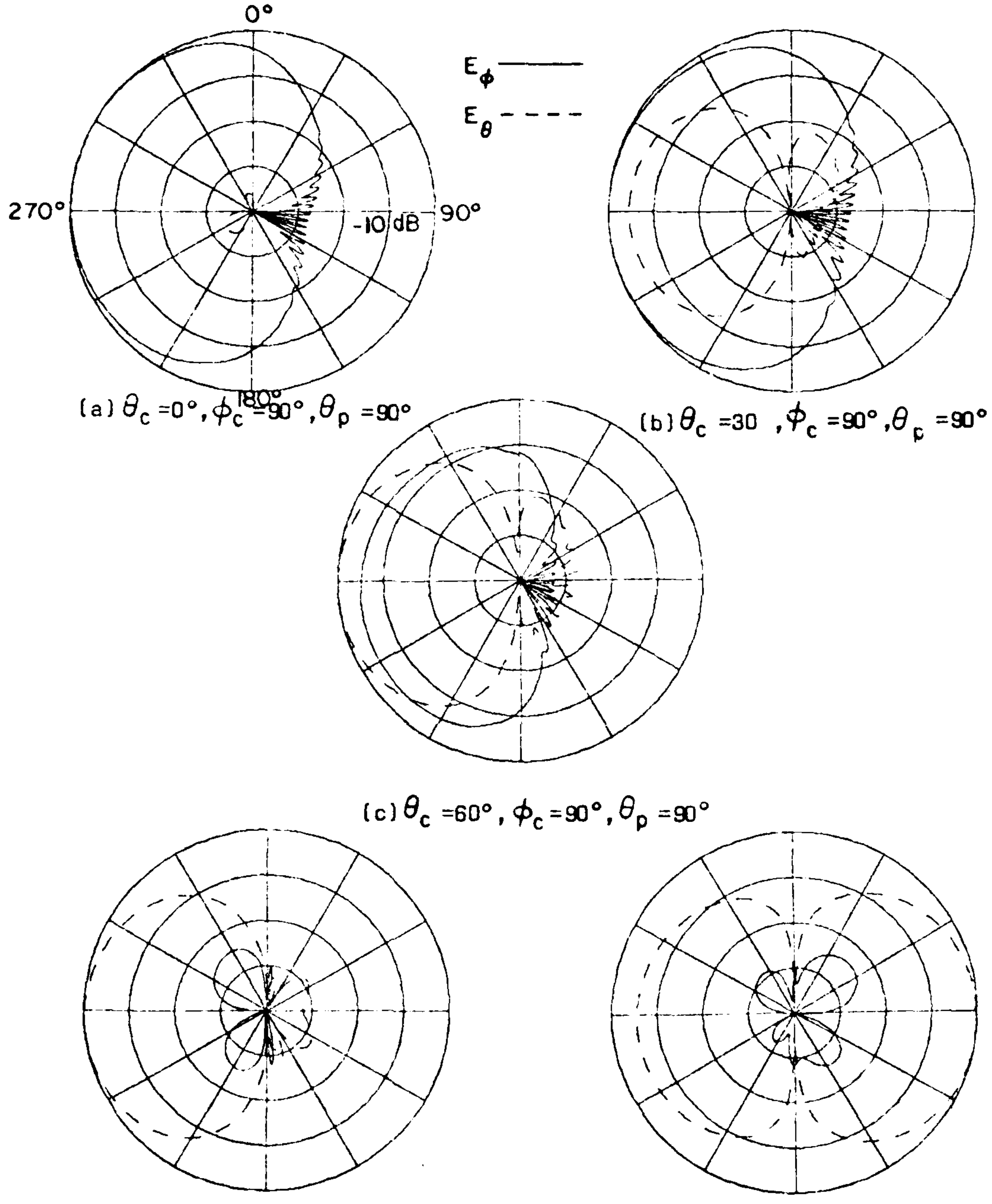

(a) $\theta_c = 0°, \phi_c = 90°, \theta_p = 90°$

(b) $\theta_c = 30 \ , \phi_c = 90°, \theta_p = 90°$

(c) $\theta_c = 60°, \phi_c = 90°, \theta_p = 90°$

(d) $\theta_c = 90°, \phi_c = 90°, \theta_p = 90°$

(e) $\theta_c = 90°, \phi_c = 0°, \theta_p = 90°$

Figure 26. Radiation patterns for an axial slot mounted at $\phi_s = 30°$, $\theta_s = 60°$ on a $2\lambda \times 4\lambda \times 10\lambda$ ellipsoid.

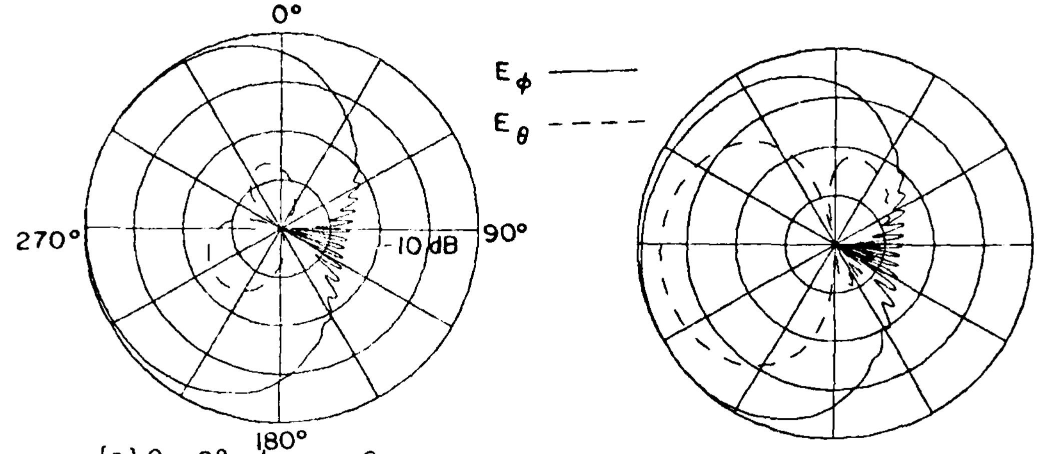

(a) $\theta_c = 0°$, $\phi_c = 90°$, $\theta_p = 90°$ (b) $\theta_c = 30°$, $\phi_c = 90°$, $\theta_p = 90°$

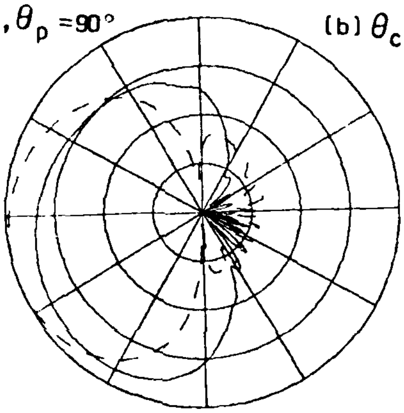

(c) $\theta_c = 60°$, $\phi_c = 90°$, $\theta_p = 90°$

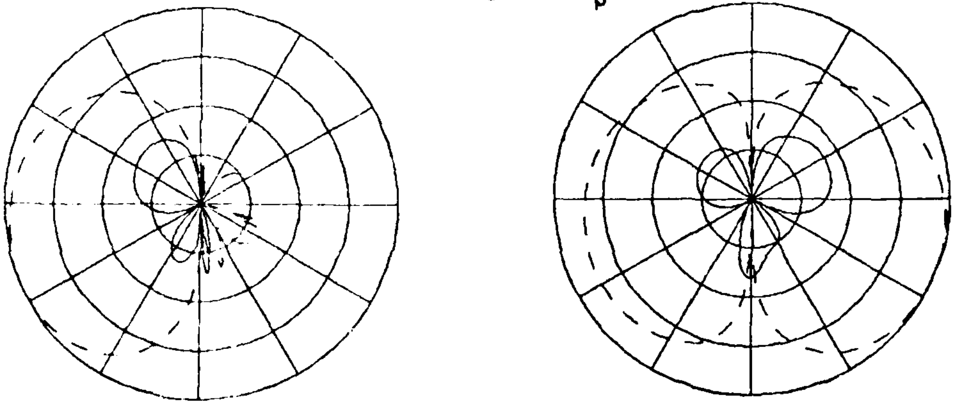

(d) $\theta_c = 90°$, $\phi_c = 90°$, $\theta_p = 90°$ (e) $\theta_c = 90°$, $\phi_c = 0°$, $\theta_p = 90°$

Figure 27. Radiation patterns for an axial slot mounted at $\phi_s = 30°$, $\theta_s = 30°$ on a $2\lambda \times 4\lambda \times 10\lambda$ ellipsoid.

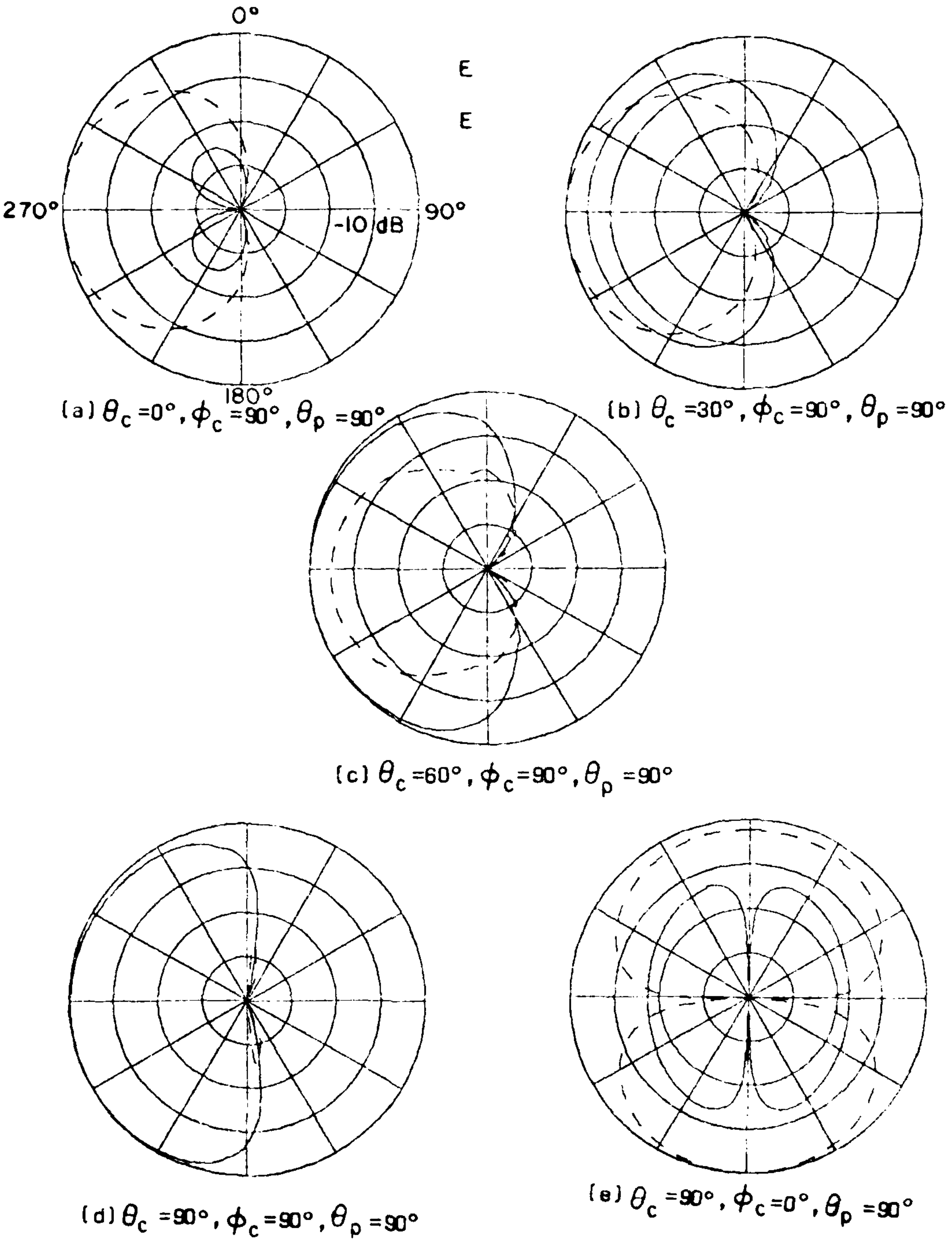

(a) $\theta_c = 0°$, $\phi_c = 90°$, $\theta_p = 90°$

(b) $\theta_c = 30°$, $\phi_c = 90°$, $\theta_p = 90°$

(c) $\theta_c = 60°$, $\phi_c = 90°$, $\theta_p = 90°$

(d) $\theta_c = 90°$, $\phi_c = 90°$, $\theta_p = 90°$

(e) $\theta_c = 90°$, $\phi_c = 0°$, $\theta_p = 90°$

Figure 28. Radiation patterns for a circumferential slot mounted at $\phi_s = 0°$, $\theta_s = 60°$ on a $2\lambda \times 4\lambda \times 10\lambda$ ellipsoid.

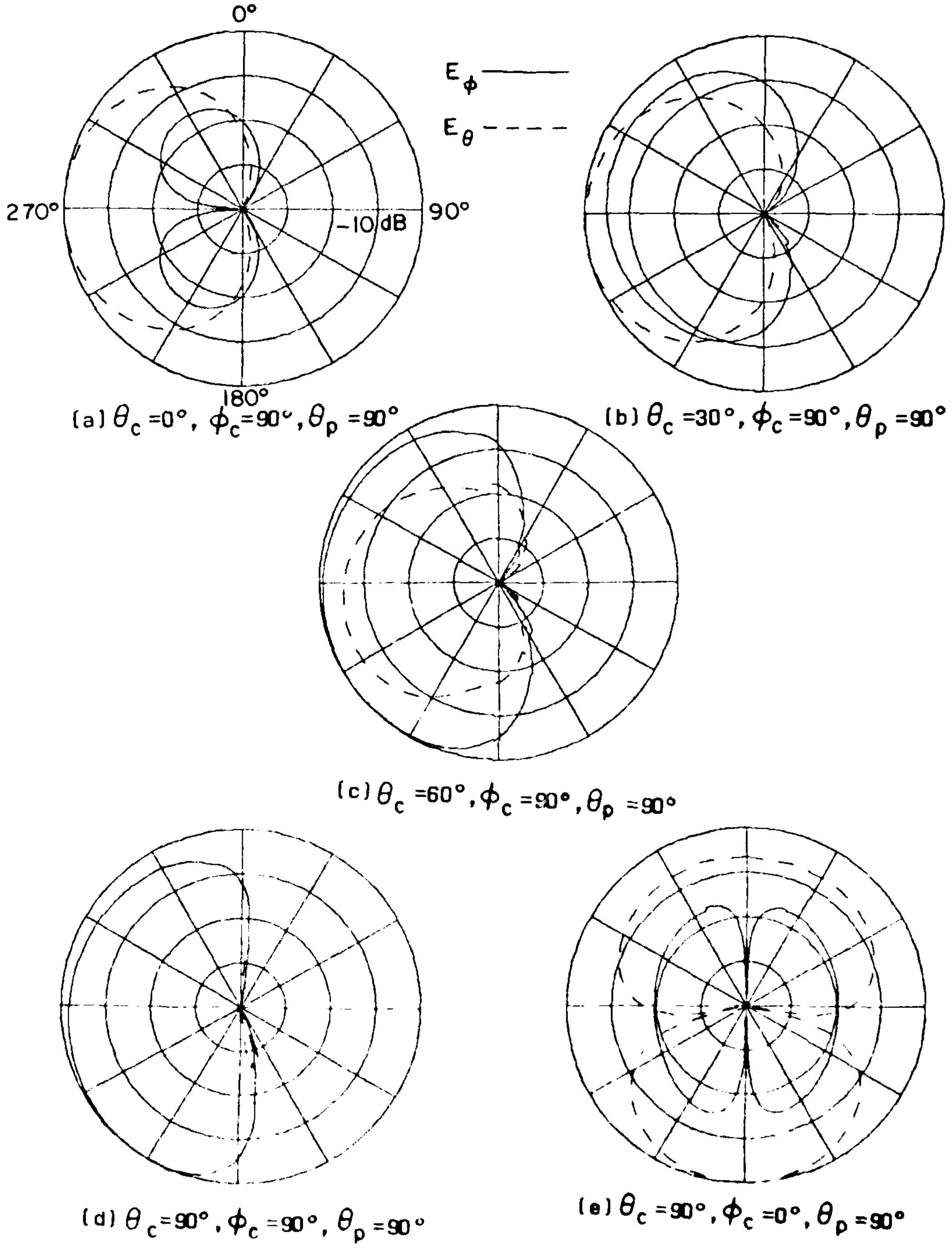

(a) $\theta_c = 0°$, $\phi_c = 90°$, $\theta_p = 90°$

(b) $\theta_c = 30°$, $\phi_c = 90°$, $\theta_p = 90°$

(c) $\theta_c = 60°$, $\phi_c = 90°$, $\theta_p = 90°$

(d) $\theta_c = 90°$, $\phi_c = 90°$, $\theta_p = 90°$

(e) $\theta_c = 90°$, $\phi_c = 0°$, $\theta_p = 90°$

Figure 29. Radiation patterns for a circumferential slot mounted at $\phi_s = 0°$, $\theta_s = 30°$ on a $2\lambda \times 4\lambda \times 10\lambda$ ellipsoid.

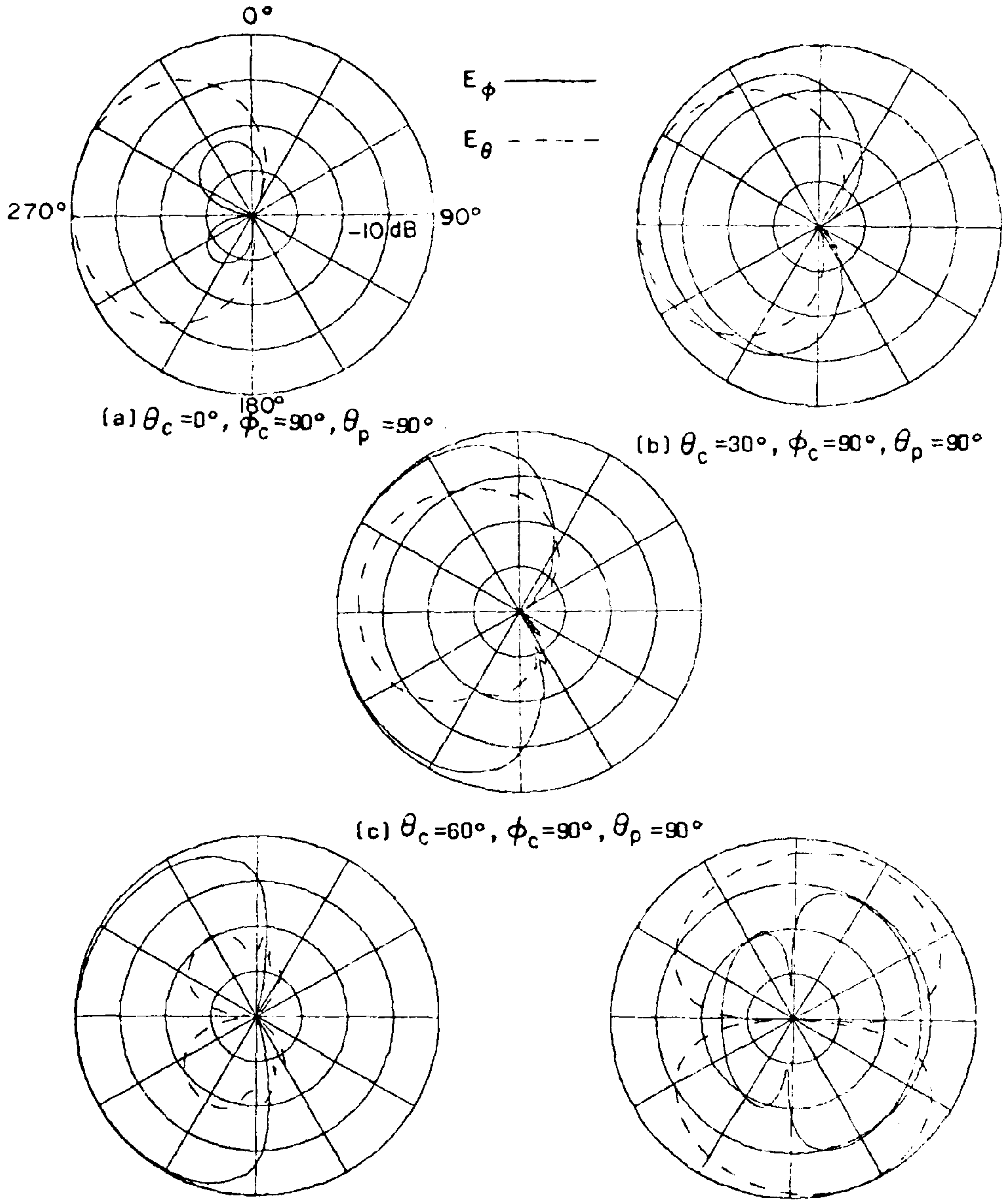

(a) $\theta_c = 0°$, $\phi_c = 90°$, $\theta_p = 90°$

(b) $\theta_c = 30°$, $\phi_c = 90°$, $\theta_p = 90°$

(c) $\theta_c = 60°$, $\phi_c = 90°$, $\theta_p = 90°$

(d) $\theta_c = 90°$, $\phi_c = 90°$, $\theta_p = 90°$

(e) $\theta_c = 90°$, $\phi_c = 0°$, $\theta_p = 90°$

Figure 30. Radiation patterns for a circumferential slot mounted at $\phi_s = 30°$, $\theta_s = 60°$ on a $2\lambda \times 4\lambda \times 10\lambda$ ellipsoid.

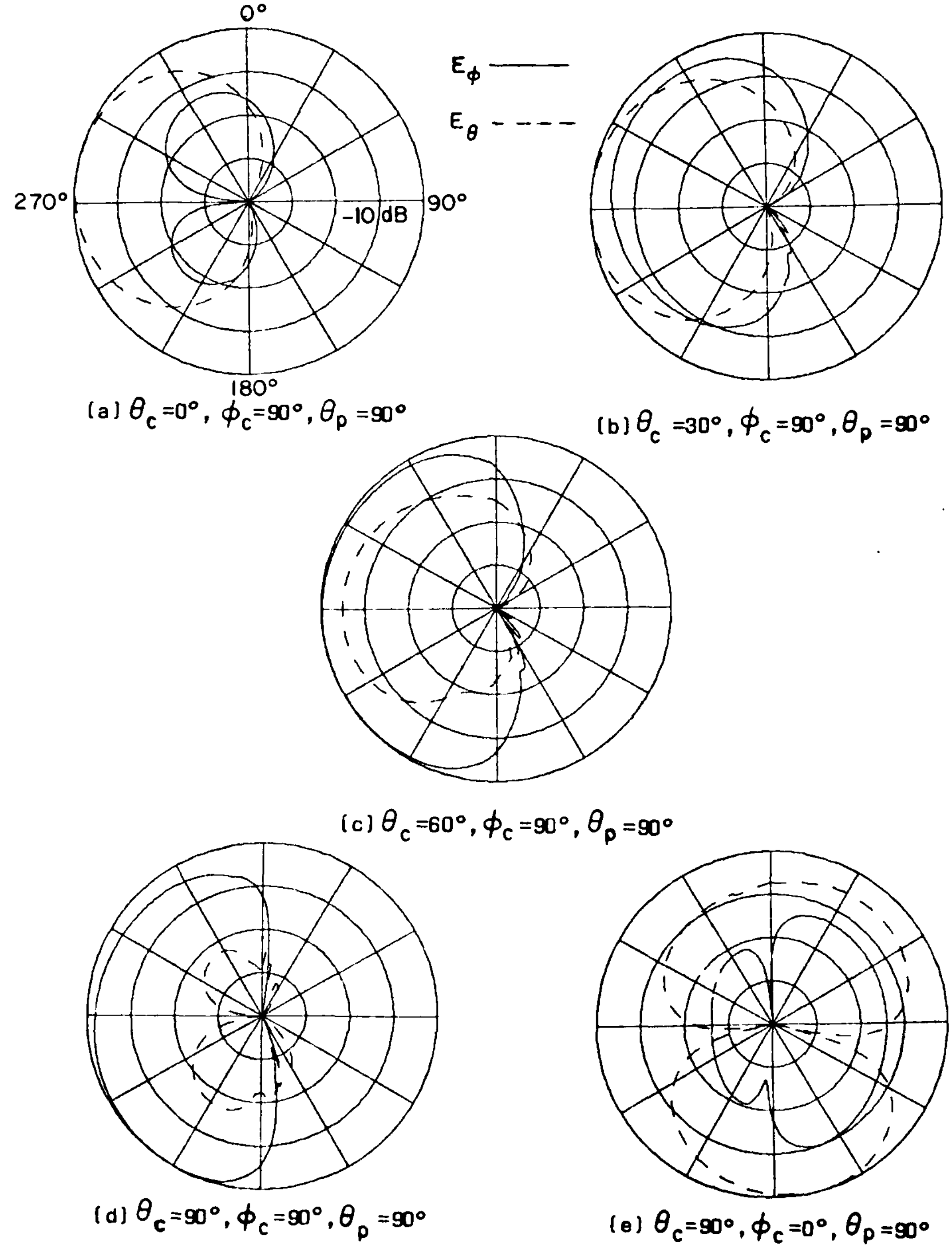

(a) $\theta_c = 0°$, $\phi_c = 90°$, $\theta_p = 90°$

(b) $\theta_c = 30°$, $\phi_c = 90°$, $\theta_p = 90°$

(c) $\theta_c = 60°$, $\phi_c = 90°$, $\theta_p = 90°$

(d) $\theta_c = 90°$, $\phi_c = 90°$, $\theta_p = 90°$

(e) $\theta_c = 90°$, $\phi_c = 0°$, $\theta_p = 90°$

Figure 31. Radiation patterns for a circumferential slot mounted at $\phi_s = 30°$, $\theta_s = 30°$ on a $2\lambda \times 4\lambda \times 10\lambda$ ellipsoid.

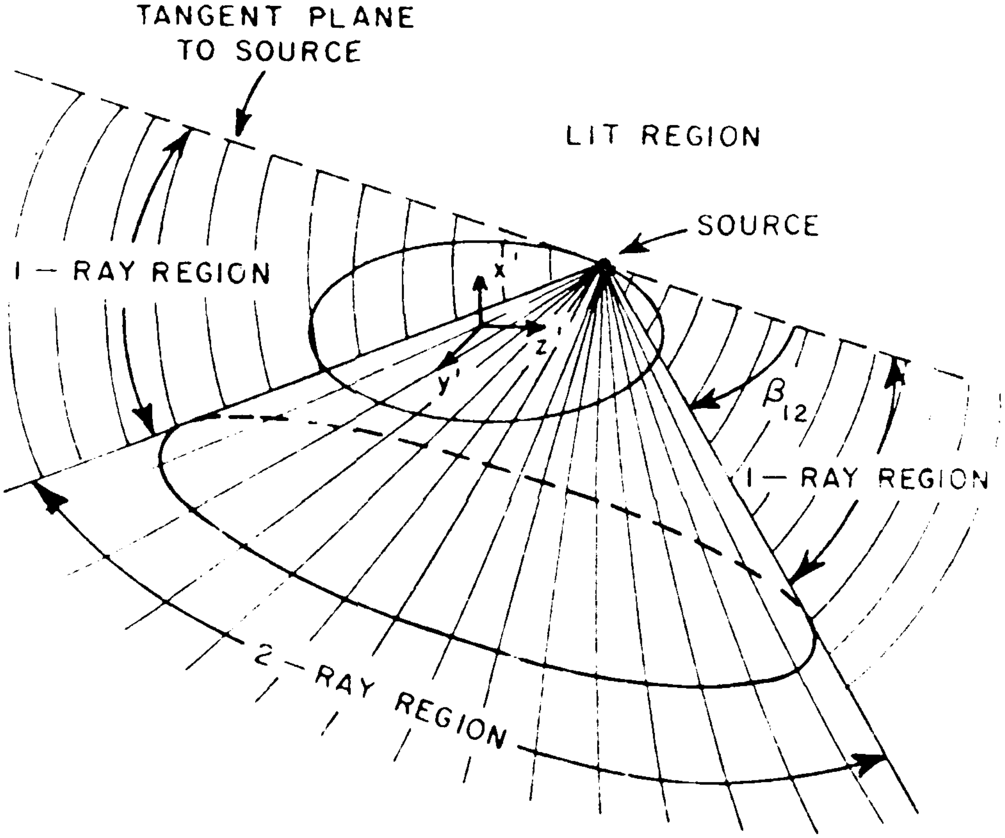
TANGENT PLANE TO SOURCE
LIT REGION
SOURCE
1 — RAY REGION
x'
z'
y'
β_{12}
1 — RAY REGION
2 — RAY REGION

Figure 32. Cone boundary used to define terms to be included in the shadow region.

REFERENCES

[1] P.H. Pathak, N. Wang, W.D. Burnside, and R.G. Kouyoumjian, "A Uniform GTD Solution for the Radiation from Sources on a Convex Surface", IEEE Trans. and Prop., Vol. AP-29, No. 4, July 1981.

[2] J.G. Kim, W.D. Burnside and N. Wang, "Geodesic Solution for an Antenna Mounted on an Ellipsoid", Report 713321-3, The Ohio State University ElectroScience Laboratory, Department of Electrical Engineering; prepared under Contract No. N00019-80-PR-RJ015 for Naval Air Systems Command, March 1982.

[3] J.G. Kim and W.D. Burnside, "Geodesic Paths for Side-Mounted Antenna on an Ellipsoid Model", Report 714215-1, The Ohio State University ElectroScience Laboratory, Department of Electrical Engineering; prepared under Contract No. N00019-81-C-0424 for Naval Air Systems Command, October 1982.

[4] J.G. Kim and W.D. Burnside, "Radiation Patterns of an Antenna Mounted on the Mid-Section of an Ellipsoid", Report 714215-2, The Ohio State University ElectroScience Laboratory, Department of Electrical Engineering; prepared under Contract No. N00019-81-C-0424 for Naval Air Systems Command, July 1983.

[5] H. Chung, W.D. Burnside, and N. Wang, "The Near Field Radiation Patterns of a Spheroid-mounted Antenna", Report 712527-2, The Ohio State University ElectroScience Laboratory, Department of Electrical Engineering; prepared under Contract No. N00019-81-C-0050 for Naval Air Systems Command, January 1980.

END

DATE
FILMED

8 — 83

DTIC